SIMPLIFYING ROBOTIC LOCOMOTION BY ESCAPING TRAPS VIA AN ACTIVE TAIL

A Thesis
Presented to
The Academic Faculty

By

Daniel Soto

In Partial Fulfillment
of the Requirements for the Degree
Master of Science in the
School of Mechanical Engineering

Georgia Institute of Technology

August 2022

SIMPLIFYING ROBOTIC LOCOMOTION BY ESCAPING TRAPS VIA AN ACTIVE TAIL

Thesis committee:

Dr. Daniel I. Goldman
School of Physics
Georgia Institute of Technology

Dr. David Hu
School of Mechanical Engineering
Georgia Institute of Technology

Dr. Frank L. Hammond
School of Mechanical Engineering
Georgia Institute of Technology

Dr. Ye Zhao
School of Mechanical Engineering
Georgia Institute of Technology

Date approved: July 15, 2022

Failure is always an option.

Adam Savage

To my family and friends

ACKNOWLEDGMENTS

Before discussing the work I've done during my time at Georgia Tech, I would first like to thank my mom, dad, and sister without whom none of this would have been possible. They have always been there for me throughout the good times and the bad and they have encouraged me to pursue opportunities that I would have otherwise overlooked. Without them and their support, I could not imagine being in the same position that I am today.

I would also like to express my deepest gratitude to Prof. Daniel Goldman. It was a strange series of events that brought us together (from an ACL tear to suddenly subbing in for another professor for a class) back in my sophomore year of undergrad and it has been quite a journey since. I am deeply grateful for all the encouragement and guidance he has given me over the years in asking the "simple" questions that yield fascinating discussions/insights and in just trying something and observing what happens. He has ingrained in me that there is no such thing as a failure in science or in life and that these events are simply opportunities to learn new phenomena or to grow as an individual.

I would also like to thank Prof. Frank Hammond for his assistance with making the robotic platform I will discuss later. His and his team's insights in making the compliant legs and in the overall manufacturing process proved to be invaluable. Additionally, I would like to thank him, Prof. David Hu, and Prof. Ye Zhao for serving on my thesis committee and helping me get through this chaotic last year of grad school.

I want to extend my sincerest appreciation to Prof. Yasemin Ozkan-Aydin for her mentorship in the field of robotics and guidance when creating and performing experiments; to Ross Warkentin for introducing me to the field of controls and being my graduate mentor when I first arrived to CRABlab; and to Kelimar Diaz for guiding me through the process of making figures, presentations, and papers for academic conferences and journals. I would also like to thank all of the CRABlab members I've interacted with during my time in the lab: Kehinde Aina, Ram Avinery, Enes Aydin, Hosain Bagheri, Joseph Brunner, Alexandra Carruthers Ferrero, Baxi Chong, Felicia Davenport, Bahnisikha Dutta, Eva Erickson,

Noah Egan, Jonathan Gosyne, Hussain Gynai, Madison Hales, Juntao He, Alex Hubbard, Christian Hubicki, Joonha Hwang, Andras Karsai, Deniz Kerimoglu, Venny Kojouharov, Shengkai Li, Marine Maisonneuve, Erin McCasky, Mason Murray-Cooper, Margot Paez, Christopher Pierce, Aradhya Rajanala, Jennifer Reiser, Tommie Robinson, Will Savoie, Perrin Schiebel, Zhexin Shen, Siddharth Shrivastava, Steven Tarr, Ian Tomkinson, Akash Vardhan, and Tianyu Wang. Each one of you has taught me in some form or another and have made the past years extremely special.

TABLE OF CONTENTS

LIST OF FIGURES

SUMMARY

Legged systems offer the ability to negotiate and climb heterogeneous terrains, more so than their wheeled counterparts [1]. However, in certain complex environments, these systems are susceptible to failure conditions. These scenarios are caused by the interplay between the locomotor's kinematic state and the local terrain configuration, thus making them challenging to predict and overcome. These failures can cause catastrophic damage to the system and thus, methods to avoid such scenarios have been developed. These strategies typically take the form of environmental sensing or passive mechanical elements that adapt to the terrain. Such methods come at an increased control and mechanical design complexity for the system, often still being susceptible to imperceptible hazards. In this study, we investigated whether a tail could serve to offload this complexity by acting as a mechanism to generate new terradynamic interactions and mitigate failure via substrate contact. To do so, we developed a quadrupedal C-leg robophysical model (length and width = 27 cm, limb radius = 8 cm) capable of walking over rough terrain with an attachable actuated tail (length = 17 cm). We investigated three distinct tail strategies: static pose, periodic tapping, and load-triggered (power) tapping, while varying the angle of the tail relative to the body. We challenged the system to traverse a terrain (length = 160 cm, width = 80 cm) of randomized blocks (length and width = 10 cm, height = 0 to 12 cm) whose dimensions were scaled to the robot. Over this terrain, the robot exhibited trapping failures independent of gait pattern. Using the tail, the robot could free itself from trapping with a probability of 0 to 0.5, with the load-driven behaviors having comparable performance to low frequency periodic tapping across all tested tail angles. Along with increasing this likelihood of freeing, the robot displayed a longer survival distance over the rough terrain with these tail behaviors. In summary, we present the beginning of a framework that leverages mechanics via tail-ground interactions to offload limb control and design complexity to mitigate failure and improve legged system performance in heterogeneous environments.

CHAPTER 1
INTRODUCTION

1.1 Overview of Field Robotics

Many of the environments humans wish to apply robots towards consist of various aperiodic heterogeneities, as shown in Figure 1.1. To cope with these scenarios, engineers have equipped "field robots" with a multitude of mechanisms to augment their mobility and obstacle handling capabilities. The majority of these augmentations are inspired from studies of biological organisms, as they are naturally equipped with the ability to traverse such complex environments [2]. Consequently, the current field of "all terrain robots" consists of a veritable zoo of robot designs where each comes equipped with certain benefits and drawbacks. Such designs are quite varied, from the number of legs to the overall size to even the control schemes employed, which emulates similar irregularities observed in nature.

In recent decades, robots have been made that cover a wide range of designs. From limbless snake-like [7, 8, 9] or worm-like [10, 11, 12] systems that wiggle through environments to myriapedal multi-limbed models that explore the mechanics behind centipede motion [13, 14, 15]. Within this spectrum, bipedal robotic systems exist which are typically applied towards working in concert with humans and operating in man-made environments. These systems are relatively stable given proper control and design [16] and thus, in more unstructured environments like those seen in Figure 1.1, they require a large amount of control and sensor complexity to achieve similar performance to humans. Quadrupeds and hexapods offer an alternative solution to these environments as they are more suited for such tasks due to their larger stability range when compared to the biped systems. Thus, such designs have received more attention for their capabilities as field robots. Considerable work has been done in developing insect-like hexapedal systems such as the RHex platform

Figure 1.1: **Natural terrains.** (A) Rough flat terrain [3]. (B) Rubble after building collapse [4]. (C) Martian landscape [5]. (D) Rough climbing terrain [6].

which takes inspiration from cockroach studies [17]. Such robots have a robust stability region due to their six actuators and by performing an alternating tripod gait, these systems can achieve high speeds while keeping the center of mass within the polygon formed by the supporting limbs. This stability benefit of a six-legged system is also the source of its main drawback as the number of actuators required for more complex mechanisms and control is scaled by 6. This increases design costs and as more moving components are introduced, more points of failures are possible. For instance, RHex uses a 1 degree-of-freedom (DoF) mechanism in its limbs but what if a roboticist wishes to implement more programmable control with a 2 or 3 DoF limb? There now would need to be 12 or 18 actuators, respectively, on the robotic system and each is a possible source of failure or overload. This brings about large power requirements if each servo motor is sufficiently strong or it results in a relatively weak system if the battery source is kept fixed. Thus, the legged design that has received the most attention in recent years has been the quadrupedal system [18]. Such a design can achieve static stability when performing a single-foot gait, where only one leg

is lifted off the ground at any point in its gait cycle, but this typically results in low speeds [19]. Instead, quadrupedal systems generally rely on dynamic stability when moving at high speeds to achieve similar performance to that of hexapods. These four-legged systems have an added benefit of being more intuitable than six-legged systems. This is because humans are more familiar with quadrupeds in our daily life and at our scale in size. Furthermore, since geometric planes are defined by 3 non-collinear points, these quadrupedal systems have a redundant support point in their fourth leg on flat ground. Thus, they offer a "middle region" between bipedal and hexapedal systems in which researchers can employ schemes developed from both biological observations and machine learning in order to figure out how best to robustly operate over complex terrains.

Two main strategies exist on these legged systems to cope with the heterogeneities present in complex terrain: environmental sensing and passive mechanical elements. Both of these schemes have aspects that are inspired by biological systems and in practice, robotic systems typically use a combination of the two strategies, albeit with a preference towards one or the other.

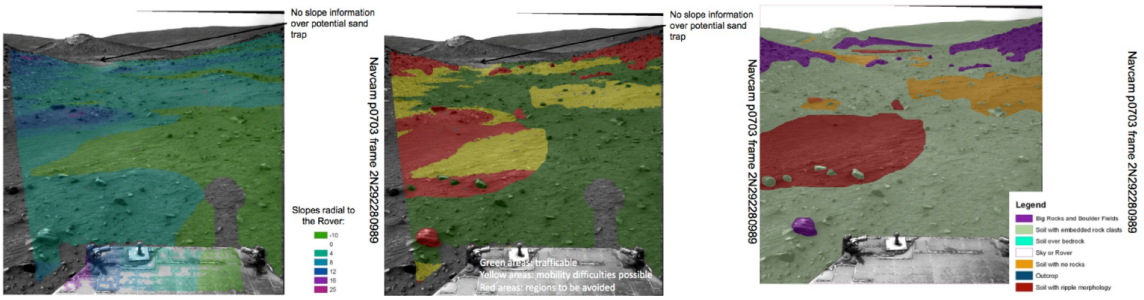

Figure 1.2: **Vision-based sensing example.** Hazard maps from the Spirit rover on Mars [20].

Environmental sensing relies on a combination of perception and cognition schemes [21] where some sensors take in aspects of the environment around the robot and then internal computation occurs to determine how that environmental information should dictate the locomotor's actions. This strategy is referred to as "task-space closed loop" since these robots use external environmental information to actively compensate for obstructions by avoiding them or through careful support placement [22, 23]. This method is inspired

by the abilities of biological systems to sense and react to their environment and in living systems, perception can be done through acoustic means such as echolocation in bats and electromagnetic sensing like in sharks, as well as several others. In recent decades, robotics has tended to favor the visual and tactile sensing methods and have employed such strategies in a variety of robots. Vision-based methods can take the form of LIDAR or stereoscopic vision to see the environment along with the distance to objects in the scene, as seen in Figure 1.2. Then, some internal controllers work to modify the robot's path trajectory to avoid or handle any observed obstructions or hazards. These methods work quite well in rovers [20] and deployed field robots [22, 24, 25]. More recent research interest has been tactile sensing and using that information to directly affect the walking pattern of the robot as this allows for more robust perception of hazards to the robot such as those seen in Figure 1.1 [23, 26, 27, 28]. An example of such a scheme and its biological inspiration can be seen in Figure 1.3 where a cockroach maintained a certain distance from the wall according to deflection detected within its antenna. Such a scheme was further verified through the use of a robophysical model [26]. The drawback of this method, however, is that it requires complex computation, control, and actuation, along with robust sensors, to be able to traverse most environments. Furthermore, the robot's speed and dynamic response capabilities suffer as a result of this bandwidth bottleneck.

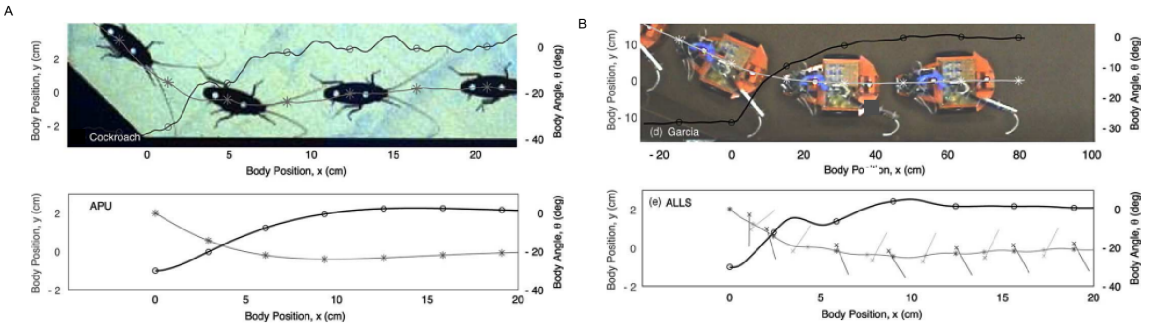

Figure 1.3: **Tactile-based sensing example.** (A) Cockroach using antenna deflection and a PD controller to follow a wall at a set distance. (B) Robophysical model verifying the proposed tactile-sensing and control hypothesis [26].

In contrast, the second locomotion strategy does not require the same level of computational intricacy to achieve comparable performance. Instead, this complexity is offloaded

to the physical design in the form of embodied intelligence [29]. This serves to augment an existing system with simple underlying motion and control, making it more robust to environmental disturbances. This method is inspired by biological systems' ability to negotiate complex terrain features faster than sensory information can be relayed to the brain [30, 31]. Such a response is called "preflexive" where the mechanisms within the limbs and body are such that their adaptation to terrain perturbations precedes internal reflexes that rely on sensory feedback and a neuromuscular response. This preflexive method, when applied to robotics in the form of embodied intelligence, offers several benefits over the environmental sensing approach such as improved energy efficiency and lower computational requirements [32]. Of major note is the near-elimination of the time delay in the robotic system's response to perturbations, thus making more dynamic movements and faster robot speeds possible. Additionally, by offloading this control to the physics of the system, it allows for the robot's computation power to be directed to more high-level tasks such as sampling environmental conditions, mapping the surroundings for other tasks, and manipulating objects.

The main drawback to this robotic embodied intelligence approach is that it can be unintuitive to the human designer on what will work well. To overcome such a limitation, recent studies have attempted to develop such designs using machine learning [33]. Generally, these devices are brought about by observing biological systems to determine what mechanisms or templates [34] enable these preflexive behaviors. For instance, based on studies of biological systems over rough terrain [35, 36], researchers found that limb compliance in the direction of loading played a significant role in the organisms' ability to preflexively react to environmental obstructions. This idea was then incorporated into various robotic designs [32] such as the robotic hexapod, RHex [17], which relies on limb compliance in conjunction with a feedforward clock-driven limb angle profile to traverse uneven terrain. Furthermore, compliant C-legs were implemented on RHex to improve its ability to climb over obstacles [37] and distribute the mechanical feedback at the limbs, like the spine does in insects and arthropods [38], another instance of embodied intelli-

gence at work shown in Figure 1.4. Along with these studies for axial loading compliance, it was also found that biological systems such as centipedes employ anisotropic compliance in the transverse direction to overcome obstacles encountered by the limbs when in the air, or within their "swing" phase [14]. This directional compliance has been implemented in robots programmatically, via actuators and control schemes [39], and physically through the use of springs to improve the robot's ability to traverse a rough terrain [14]. These studies demonstrate the impact that different limb mechanisms have on overall robot performance but this design approach is not limited solely to robot limbs.

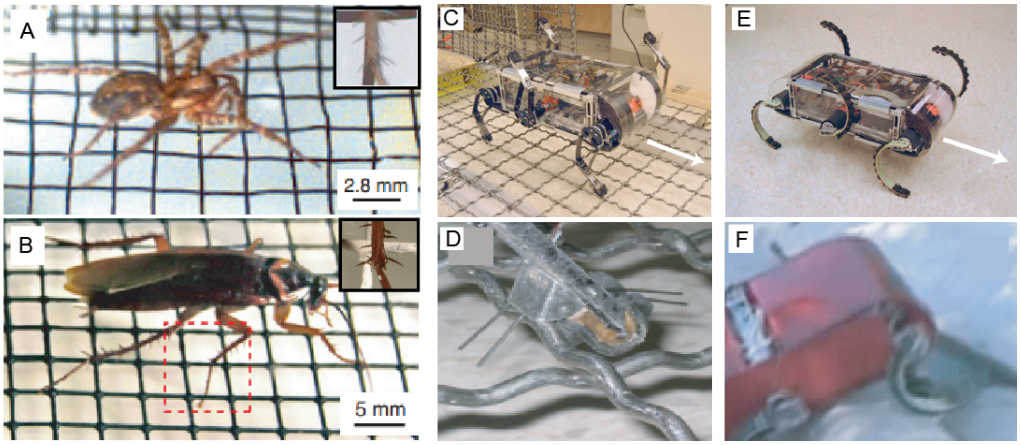

Figure 1.4: **Embodied intelligence via distributed mechanical feedback at feet.** Collapsible spines on a (A) spider and (B) cockroach facilitate motion across a mesh [38]. (C) RHex model using compliant linkages for legs and equipped with collapsible spines (D) to enable motion across a mesh. (E) RHex with C-legs that distribute contact over hazardous terrain (F) to improve performance.

An embodied intelligence design approach can be applied to other aspects of the body, such as the shape [40, 41], flexibility, and the methods of actuation. These features serve to simplify the control complexity needed for robust locomotion by introducing passive elements rather than active components. For instance, compliant body joints were incorporated into a centipede-like robophysical model to augment its ability to negotiate the transition between flat ground and inclines [14]. This flexibility within the body joints demonstrates how passive elements can offload computation from the "neurological" controller to the mechanical design. Another example of such a concept is the undulatory robot

shown in Figure 1.5 A. This design is based on observations of snakes in lattices and uses muscle-like morphology to traverse multi-post arrays via emergent passive mechanics (see Figure 1.5 B-D) [42]. In this study, the actuation of the body wave was accomplished via strings that acted like "tendons" to provide tensile loading while passively deforming in compression. Such a method allowed for robust locomotion through 2D obstacled environments, as shown in Figure 1.5 E. This serves as another case where the tasks done by a robot with a straightforward mechanical design and a complex internal control scheme [43] could be similarly accomplished by a robot with a simple control scheme and a more mechanically complex physical design.

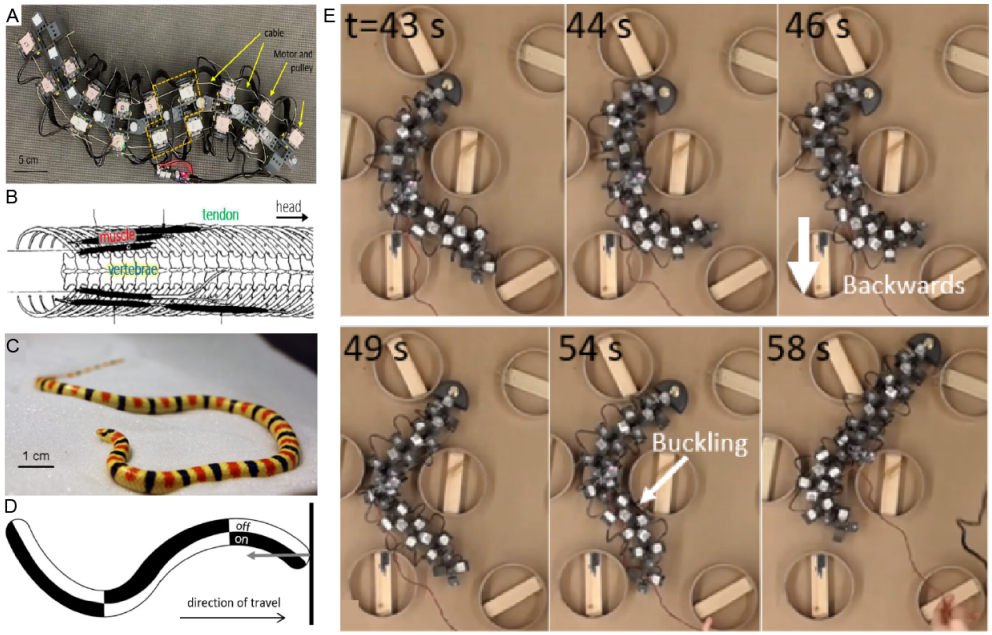

Figure 1.5: **Embodied intelligence via muscle-like actuation.** (A) Robophysical snake model that uses tendons to actuate the body undulation [42]. (B) Simplified snake anatomy showcasing the musculoskeletal system that drives lateral body bending in snakes. (C) *C. occipitalis* on model desert sand. (D) Cartoon depicting muscle activation and compliance. (E) Snapshots of robot demonstrating passive buckling and reversals to traverse a cluttered lattice.

Despite the benefits the task-space control methods have in avoiding environmental hazards and the improvement that the embodied intelligence design approach has towards robust locomotion, robots are still susceptible to failures over some complex terrains. These situations and hazards can take many forms and can be brought on by several factors. For

instance, there are the failures incurred by size/design when locomoting over unstructured environments, such as those shown in Figure 1.1 B&D. Large walkers can clear the gaps and obstacles present in these environments. However, they are prone to tipping over and to collapsing the underlying structure due to their weight, both of which result in damage to the locomotor. In contrast, small walkers are lighter and less prone to damaging themselves or their environment, but are also less likely to clear the gaps and obstructions. We posit that there is a moderate size and weight class where the robot is unlikely to collapse a structure or be damaged from falling, while still maintaining the ability to clear most obstacles and gaps. However, this "middle" category of robots can have limb dimensions that are of comparable size to the obstructions and holes being traversed [44]. In this regime, stalling or "trapping" events begin to occur [38] where a limb falls into a cavity and is unable to be easily removed. This form of locomotor failure is detrimental to robots using either motion strategy and can be encountered across many environments. This condition of having a limb trapped and causing damage to the locomoting system is not specific to robots either and can be observed in biological systems like lizards and insects. However, these organisms can recognize when they have an appendage stuck and can utilize complex limb dynamics and the rest of their body to either free the limb or remove it. Therefore, field robots should have some comparable method of detecting and freeing themselves when they have fallen into a trap in order to improve their all-terrain capabilities.

1.2 The trapping condition and possible solutions

These "trapping" scenarios depend on both the locomotor kinematic state and the local terrain configuration. For instance, a foot-sized hole is hazardous to a legged system when it is encountered by a limb pushing off the ground but that same hazard is harmless when the limb is in its swing phase. Due to this geometric coupling, these situations prove to be quite challenging to predict and overcome. Generally, the strategy is to avoid areas where such a scenario can occur [20] as seen in Figure 1.2. However, this is not always feasible since the goal location could reside in a hazardous region or the risk could be hidden from

plain view. The Spirit rover is an example of the latter since it ended its mission when a wheel fell into an unperceived hazard of soft sand beneath a thin layer of normal-looking soil [20]. The rover was unable to extricate the wheel from this trap and it eventually was reclassified as a stationary research platform, losing its ability to function as a mobile robot. Being detrimentally susceptible to visually imperceptible hazards is a common problem amongst all robotic systems currently deployed and thus, work has been done on how to adjust walking patterns to "probe" the terrain as the robot walks [23]. However, this is but one of many scenarios that can cause trapping and so, it further demonstrates a need in robots for a means of self-extrication before catastrophic damage occurs.

Trapping failures are induced by the interplay between the physical state of the locomoting system and the relative terrain conditions. Thus, modifying the surroundings or changing the state of the locomotor could serve to mitigate such interactions. To do the former would signify "remodeling" the environment to better suit the robotic system. This approach works well in flowable mediums such as sand where the media can effectively change from being an elastic solid to a frictional fluid [45]. In a more rigid environmental setting, this strategy can be viewed as moving the obstruction. For example, if a leg was pinned between the ground and a rock, "modifying the environment" would be equivalent to "moving the rock" in this scenario. However, this strategy is not suitable for all locomotors as the power cost associated with performing such a task could be larger than the feasible output of the system.

The other option for mitigating terrain trapping failures is by modifying the physical state of the locomotor with respect to its local environment. This can be done via some form of proprioceptive sensing to determine which appendage is trapped and then using the remaining limbs in some way to release that leg. This is how biological systems react to traps since these organisms possess a large amount of sensors and degrees-of-freedom in which to actuate their already compliant bodies. However, achieving such a level of self-awareness and motion-complexity in an artificial robot system is currently not feasible for deployed field robots. We posit that this complex, case-by-case sensing and action that

organisms perform can be emulated to an extent by including a separate non-locomotory appendage that follows an open-loop strategy or a simple closed-loop control scheme. This mechanism would serve to disrupt the robot's state relative to the terrain, thus freeing it from a trapping region. This method is feasible since such an approach is quite similar to the concept of embodied intelligence discussed previously, where computational complexity in the robot is simplified by offloading the control to the mechanics of the system. In this case, the inclusion of an actuated mechanism is simplifying the necessary control strategy for the limbs. This methodology has been applied to robotic systems before where the limb control was made more robust by offloading certain forms of stabilization/control to other parts of the body. These approaches have typically been in through body actuation [46, 47] or, more notably, in the form of a tail which serves as inspiration for how to best handle these trapping failures.

1.3 Tails in locomoting systems

Tail designs in robotic systems can be grouped into two categories: in-air and substrate-contacting. Applications of the former typically rely on conservation of angular momentum and are used to reject some form of disturbance or inertially reorient the robot while falling. An example of this disturbance rejection is exhibited by the MIT cheetah robot swinging its tail to avoid toppling over when hit by a swinging mass [48]. However, most instances of in-air tail usage are to assist the locomotor as it is falling from some height. This method takes inspiration from organisms such as cats and lizards which use their tails when jumping to reorient their body as seen in Figure 1.6 A [49]. This strategy has been emulated in several robots [50, 51, 52] such as the XRL [53] and Tailbot [54] shown in Figure 1.6 B&C performing such a maneuver. While this method of tail use works quite well with disturbance rejection and reorientation, it would not be effective at properly handling trapping failures. In these scenarios, the tail must alter the robot's physical state, and so, the tail would need to be massive to generate the necessary torques. Therefore, this type of tail mechanism would be infeasible for most robotic systems, making it an unlikely candidate

to resolve trapping in field robots.

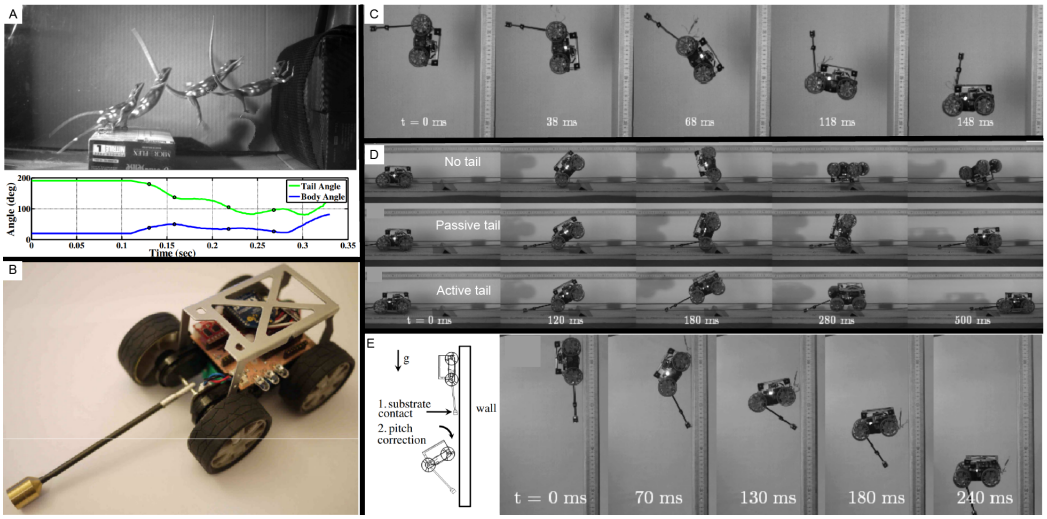

Figure 1.6: **Tail use to augment locomoting system.** (A) Lizard jumping off a low-friction surface to land on a wall [54]. It maintains a relatively constant body angle (blue) by using its tail (green). (B) Robophysical model, Tailbot, consisting of a car with a tail that has a mass at the tip. (C) Tailbot inertially reorienting itself in mid-air. (D) Tailbot encountering an obstacle without a tail (top), with a passive tail (middle), and with a tail maintaining an angle relative to the body. By using the tail, the robot avoids catastrophic pitch-back failure. (E) Tailbot reorienting itself by pushing off a wall with its tail.

In the second category of mechanisms, the tail acts in direct contact with the ground to induce several behaviors. Within this group, there exist static and dynamic strategies which serve to augment the locomotor capabilities. For example, in Figure 1.6 D, Tailbot encountered an obstacle that caused catastrophic pitch-back failure in the non-tailed system as seen in the top row. By adding the tail and dragging it behind the body, the robot mitigated the perturbation's effect (middle row). Furthermore, by maintaining a set angle relative to the body, the tail eliminated the pitch-back entirely (bottom row). This and others [55] are instances of static substrate-contacting tail strategies. In the dynamic regime, there are several examples of a tail's benefit in a granular medium, acting as both a means of obstacle navigation [56] and propulsion [57]. However, this appendage also works well over more rigid substrates, as seen in Figure 1.6 E. Here, Tailbot impacts a wall to induce a pitch correction that would be otherwise infeasible without substrate contact. Another instance of a dynamic tail strategy in a rigid environment includes impacting the ground to

steer a locomoting robot, accomplishing rapid 90° turns in the process [55]. In this study, a relatively weak servo motor was able to affect the trajectory and the physical kinematic state of the overall robot by tapping against the substrate. As such, this method of tail use could serve as a possible means to handle trapping scenarios.

We posit that, by altering its physical state, a robot could effectively deal with trapping failures. The substrate contact method is appropriate for this task, as the Tailbot and LoadRoach studies demonstrate that a tail on the ground has the capability to affect the entire robot [54, 55]. However, in heterogeneous environments, such a method is susceptible to the randomness present in the terrain, making it unclear how best to implement a tail. Therefore, a study must be done on effective tail contact strategies to overcome the complex dynamics of this coupled terrain-locomotor trapping event.

To probe the question of how to use a tail to overcome trapping failures, different testing methodologies can be adopted. For instance, experiments could be done on biological systems to explore how they utilize their tails in such scenarios. However, as discussed previously, these organisms have a vast degree of sensor and actuator complexity so it is likely that they would not use their tails in the first place, relying instead on their compliant body and limbs. A real-world machine learning approach could be performed instead to work out how best to use a tail in various terrains. Such an approach avoids issues with friction and collision models affecting the learning process since the world acts as the physics engine. Such a method has yielded success in previous studies where robots learned gaits to effectively operate across many environments [58, 59, 60]. However, this approach does not typically offer insight into why the learned strategy works and can be subject to overfitting on the training set.

By determining whether a tail can overcome trapping, there should be an increased comprehension of how these under-studied failure scenarios occur and why the tail helps. This suggests that a "robophysical" approach is best suited for such a study. In this field of research, certain aspects of a model are systematically tested to build up the experimentalist's understanding of the governing mechanics [61, 62, 63]. An added benefit of this

robophysics method is that it arms the researcher with a better understanding of the emergent dynamics of the system. As such, new controllers and observers can be made that leverage the inherent physics to make the system behave as desired [64, 65]. Therefore, this robophysical approach is key to investigating how and why trapping failures occur and how a tail can be used to overcome such scenarios to augment deployed field robots.

1.4 Objective

To determine how a tail can perform substrate contact to mitigate trapping events requires a systematic approach to understand the dynamics involved. As such, three key items are required:

1. A robust, easily repairable legged system that can be augmented with a tailed appendage. This robophysical model's control must be robust such that it can be programmed to follow explicit instructions while being subject to the randomness of the terrain and nonlinearities caused by stalling events.

2. A rough terrain course capable of systematically producing trapping events with the legged model.

3. A tail that can be easily attached to the legged system that is capable of providing sufficient torque to affect the robot.

Chapter 2 is dedicated to the development of these three items to facilitate robophysical testing and chapter 3 discusses the different control schemes for the appendage and the change in performance across the terrain. Chapter 4 serves to conclude on the results presented in chapter 3 and to propose future work to further this investigation.

CHAPTER 2
MATERIALS AND METHODS

2.1 Legged robot

We emulated the RHex design as it is a system that leverages passive mechanics and feed-forward control to walk. This serves to highlight how the tail can offload control complexity from the limbs when encountering traps. However, we used four limbs rather than the standard six. This was to reduce the number of points of mechanical failure and to further probe the capabilities of such a system [66]. The resulting RQuad robot (length and width = 27 cm, limb radius = 8 cm) is shown in Figure 2.1 A&B with certain portions highlighted. The following subsections serve to further detail aspects of the robot design and control.

2.1.1 Limb Design

Each limb, shown in Figure 2.1 C, is composed of two parts: an aluminum motor shaft coupler and a flexible polyurethane resin leg component. The coupler attaches to the motor shaft via set screw. This component was used since the torque generated by the actuator during trapping events would be likely to shear most compliant materials over time given a press-fit and we know that compliance plays a significant role in robust locomotion. The flexible portion (leg) connects to the aluminum coupler via a slot and three screws that go into partially-threaded holes (clearance fit on one slot wall, threaded on the other). This results in the screws effectively clamping onto the legs, further distributing the stresses away from the motor. To make the legs, we 3D printed the desired model and then cast it in silicone. Once the silicone finished curing, we cut the block in half to remove the printed part, resulting in a mold of the component (see Figure 2.1 D). The polyurethane resin was then poured into the silicone to cure and once removed, we opened the holes for the slot screws and removed the leftover material (flash) from the molding process.

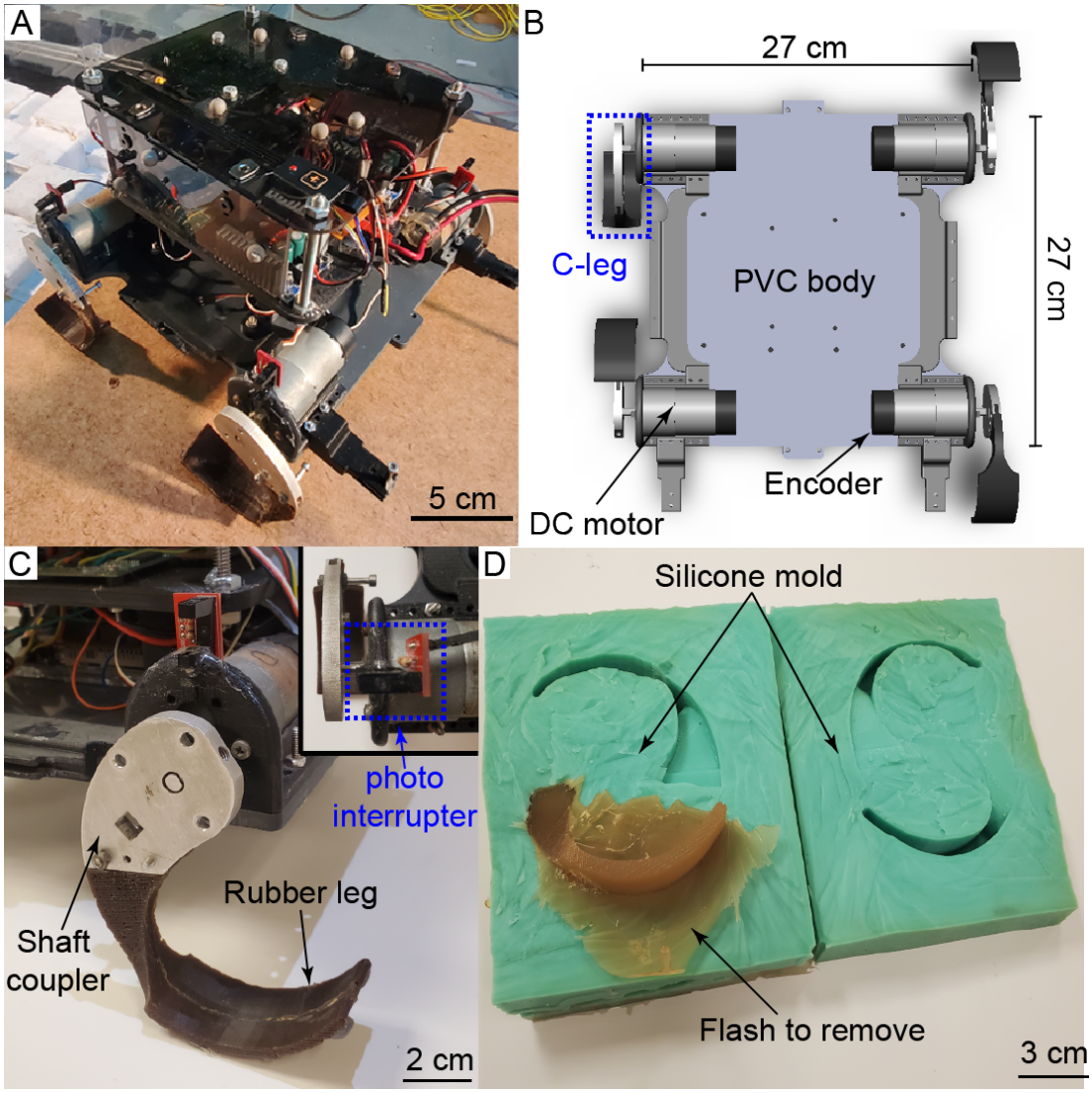

Figure 2.1: **Robot and limbs** (A) Physical robot model (B) Simplified computer model with lengths and materials specified. (C) Physical robot limb with the photo interrupter specified in the upper right panel. The pin at the top of the panel passes through the gap in the sensor, triggering a digital signal which is observed on the microcontroller.(D) Two part silicone mold used to make the legs. The flash is removed after extraction from the mold.

2.1.2 Electronics

The limb actuators are Pololu 37D 70:1 gearmotors which come with a relative encoder. These motors have a top speed of 2.5 rev/s and a stall torque of 27 kgF·cm with an associated current of 5.5 amps. A power supply tether was used for these experiments, which can be replaced with an appropriate battery in future projects. We used an Anmbest buck

converter to ensure the 4 motors were supplied with 12 volts with a maximum current rating of 22 amps. The motors were separated into 2 ipsilateral pairs and each pair was driven by a Pololu Dual VNH2SP30 Motor Driver Carrier MD03A. This driver is capable of supplying the actuators with the high power necessary for testing failure conditions, while also offering rudimentary current sensing for each motor (not used within the scope of this work). To monitor the overall power consumption, we placed a Pololu ACS714 Current Sensor Carrier on the line directly from the power supply before the buck converter. An Arduino Due serves as the "limb microcontroller" for this robot and it operates the motors and monitors the associated sensors. To avoid voltage ripples from the motors affecting the logic board, the Due is powered from a separate on-board 3.7 V battery that is boosted to 5 volts by a Pololu 5V Step-Up Voltage regulator. Since each motor comes with a relative encoder, we placed a photo-interrupter (see Figure 2.1 C panel) on each actuator to provide an absolute position, thereby avoiding encoder drift over time. The signal from this light-based sensor was subject to bouncing and false positives during preliminary testing. To reconcile the bouncing issue, we included a basic sensor filter in the code to check whether a positive reading had been registered in the past 1.5 milliseconds and if so, disregard the new reading. Additionally, to resolve the false positive issues, we implemented a rudimentary sensor fusion where a new photo-interrupter signal was not registered unless its corresponding encoder read as being roughly three quarters of the way through its cycle. Once a true reading was registered, the internal encoder value would reset to zero while all other position-related values were reset such that their differences were maintained with respect to the actual encoder.

2.1.3 Control

Each limb rotates according to an angular trajectory known as the Buehler Clock [17], which consists of a fast and a slow region (Figure 2.2 A) where the slow region is generally when the limb is in contact with the ground. Each motor follows the assigned motion profile via a feedback control scheme detailed in Figure 2.2 C. This limb control consists

of two cascaded PID control schemes with the inner velocity loop running at 4 ms. This is five times faster than the external position control which outputs a correction term for the velocity control loop based on the difference between the actual and setpoint positions. To calculate the actual velocity, a numerical derivative of the encoder values was performed using microseconds and ordered such that bitwise precision was maintained. By using a cascaded set of control loops, smooth tracking of the desired curve was ensured without significant drift. To generate the desired setpoint profile, the following functions were used:

$$\theta_{i,d}(t) = \omega_{i,d}t \quad , \quad \omega_{i,d}(\theta_{i,d}) = P_i + \begin{cases} \omega_s & \theta_{min} \leq \theta_{i,d} < \theta_{min} + \phi \\ \omega_f & otherwise \end{cases} \tag{2.1}$$

Where ω_s and ω_f are the slow and fast velocities, respectively, and their formulas are detailed in the appendix. Subscript d indicates that this variable is the desired reference signal used in the control scheme in Figure 2.2 C. To prevent significant windup from occurring when a trapping event occurs, $\theta_{i,d}$ was modded by 1 whenever $\theta_{i,d} - \theta_i > 1$ which signifies that the setpoint position has done a full revolution with respect to the actual limb. We implemented this position-based scheme rather than a clock-driven method since it results in a simple yet robust implementation of the angular trajectory that is insensitive to motor stalling. The robot locomotes by following a gait pattern (i.e. phasing the limbs relative to each other in time) [67]. An example pattern for a diagonal couplet gait is shown in Figure 2.2 B, where the symmetric phasing ψ_{lat} (phasing between limbs on the same side) is 35% and the asymmetric phasing ψ_{opp} (phasing between the pairs of limbs on either side) is 50%. By setting the initial position of each motor to correspond to a snapshot in time of a desired gait and by using the setpoint functions detailed in Equation 2.1, the robot can easily emulate the prescribed pattern as time goes on, assuming no disturbances that will significantly perturb $\theta_{i,d}$.

However, as the topic of this study is the trapping condition, stalling behaviors are to be expected and those will constitute significant disturbances to the desired setpoint profile and gait pattern. To resolve this, a method of enforcing the relative temporal phasing

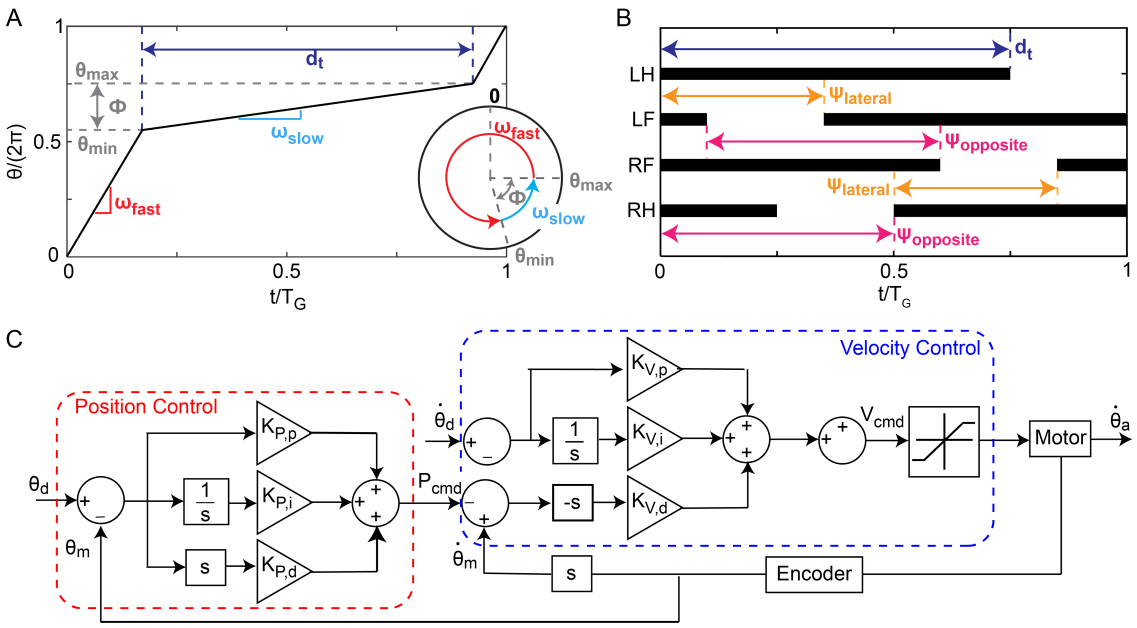

Figure 2.2: **Control schemes.** (A) Motion profile for limb rotation. Trajectory (black line) described by two speeds: fast (red) and slow (blue). Slow region described by the stance phase (gray) and the time spent there is described by the duty factor (purple). (B) Gait diagram showing relative limb phasing. Black is when the limb is in the slow region and has a length equal to the duty factor (purple). Each lateral and opposite pair is phased by ψ_{lat} (orange) and ψ_{opp} (pink), respectively.

between the limbs is needed while also keeping the control decentralized so as to fit best with Equation 2.1 (i.e. not a central pattern generator). Inspired by reflex chains seen in simple organisms and robots [27, 28, 68], along with the efficiency displayed by decentralized control algorithms to generate robust locomotion [69], and guided by our desire to systematically test different gait patterns, we developed a state feedback control scheme to coordinate the limb motions. The details of this scheme and its implementation are in the appendix but in short, it effectively results in each motor looking at its neighbors to adjust its own setpoint velocity (seen in Equation 2.1 as P_i) until the desired gait pattern phasing is achieved.

For overall system implementation, we randomized the order in which motor commands were sent each code cycle. This was to prevent drift accumulating on the final motor in the sequence, which was a significant issue in preliminary tests. Finally, to ensure failure events would not cause permanent damage with every trial, we placed a "kill" switch

on the robot. If a limb failed to complete a revolution within two gait cycles (5 seconds), this indicated a trapping event and the robot shut down, ending the trial.

2.2 Terrain

To model unstructured terrains and trapping conditions, we constructed a stepfield of length 160 cm and width 80 cm (model shown in Figure 2.3 B). This is a common approach for modeling obstacle-laden environments [17, 36, 70] and it consists of placing a collection of blocks randomly across a grid where each block height is chosen from some random distribution. For this study, since the goal was to induce trapping, we desired a distribution that:

1. prioritized having blocks of tall and short heights;
2. kept the range in heights feasible for the robot to climb;
3. contained blocks within the tall and short bounds so that the robot was continually perturbed.

Given these goals, we used an inverted normal distribution whose associated equations are detailed in the appendix. It takes as inputs a mean μ, a standard deviation σ, and bounds β. For the purpose of this study, these values were normalized by the limb radius (8 cm) for the distribution generation and we used a mean of 6 cm (0.75 leg radius), standard deviation of 1.6 cm (0.2 leg radius), and bounds of 6.4 cm (0.8 leg radius or 4 times the standard deviation). Each block was given a 10 by 10 cm footprint to scale them to be roughly a third of the robot's body length and width. Therefore, there were 128 blocks in total and the resulting distribution is shown in Figure 2.3 A as the red line with 11 bins for the heights.

With the heights and dimensions chosen, the blocks were then placed across the 2D grid such that, starting from the center, the tallest block was placed and then surrounded by the shortest blocks available and then those short blocks were surrounded by the tallest blocks

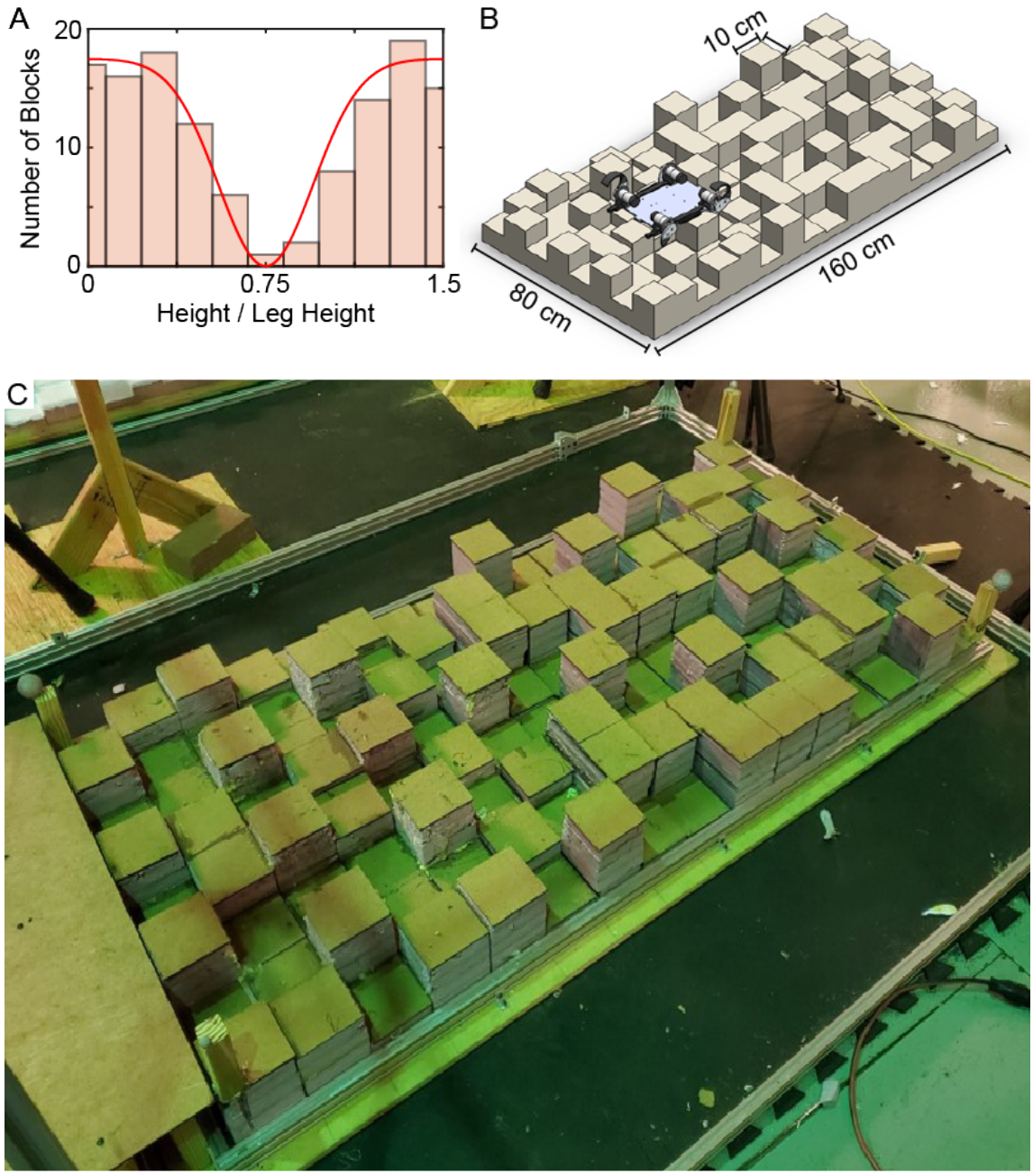

Figure 2.3: **Rough terrain.** (A) Inverted normal distribution used to obtain block heights. (B) Design of terrain with simplified robot model. (C) Physical terrain model.

available. This placement pattern continued outwards from the center in a counterclockwise spiral when looking at the terrain from above. This method resulted in a terrain that starts with alternating blocks with shallow height disparities that get progressively larger as one moves along the terrain and towards the end, the block patterns become more unstructured

with moderate height differences.

To create the terrain model shown in Figure 2.3 B, we stacked several inch thick insulation foam sheets and cut them into 80 by 10 cm strips. We placed these boards under a waterjet to carve out the 16 desired geometric profiles. Then we placed the finished strips on a wooden board and glued them into place. To prevent damage to the foam interior, we placed a 3 mm thick wooden square on each block. The finished terrain is shown in Figure 2.3 C with a flat board on the left for the robot to start from and IR reflective markers at the corners for tracking purposes.

2.3 Tail

For the active tail, we attached an aluminum beam (length = 17 cm, width = 2.7 cm) and two Savöx high torque servo motors (operated at 7.4 V, max torque of 40 kgF·cm) to the robot (Figure 2.4 A). The overall tail weighs 0.4 kg and at its end is a triangular pad for ground contact and tracking. The tail and its components are shown in Figure 2.4 C. Nylon rods act as rolling supports to distribute the reaction forces away from the yaw servo and a steel pin serves a similar function for the pitch servo. Acrylic skids were placed on the underside of the aluminum beam to mitigate instances where the tail bottom gets caught on an obstacle. A strain sensor consisting of 4 strain gauges and a full Wheatstone bridge was mounted onto the beam. For this study, this sensor was not utilized in any control schemes or analysis but it could serve as a source for future work.

The tail was controlled via an Arduino Pro Mini that had serial communication capabilities with the Due running the limbs. However, this communication channel was not used in this project as the goal was to study how a tail could offload the control complexity requirements for the limbs. Thus, the tail was not explicitly coordinated with the legs. This serves to make this study's results more applicable to deployed robots as it implies that an active "lever" can be attached to a locomotor without needing to rewrite the existing code.

Within this study, the tail was free to move in the yaw direction as seen in Figure 2.4 B. This degree of freedom can be active in future work but the goal here is to investigate the

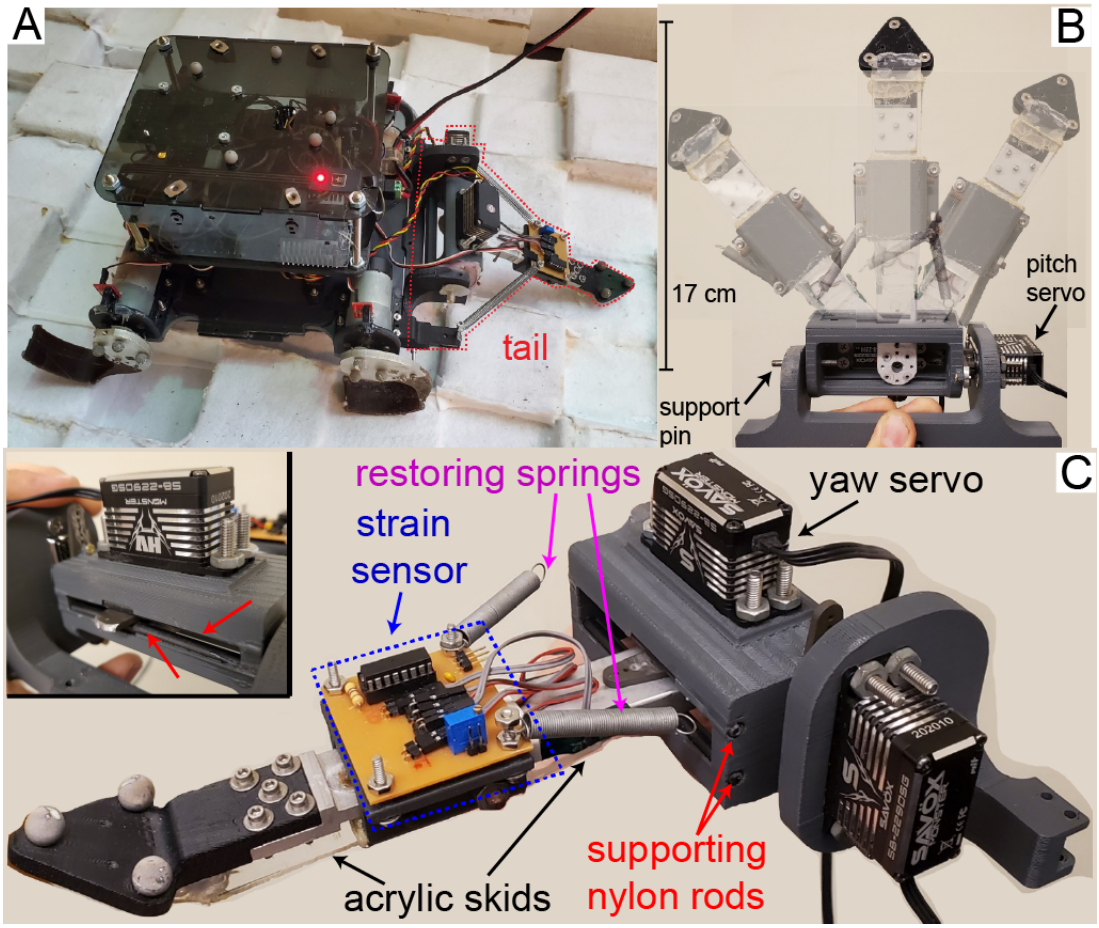

Figure 2.4: **Physical tail figure.** (A) Robophysical model with tail. Red dashed lines outline the tail. (B) Tail with its range in yaw shown along with dimensions and certain components highlighted. (C) Tail with annotations highlighting key components.

simplest form of effective control. As such, restorative springs were used such that the tail returned to the center after yaw movement. The mechanism's motion was actively actuated along the pitch direction, varying the maximum tail angle (β_{set}) relative to the robot body from 0° to 90° (Figure 2.5 A).

2.4 Experimental Procedure

We implemented three tail strategies in this robophysical study: static pose, periodic tapping, and load-triggered tapping. The static tail strategy consists of maintaining a set angle relative to the body. This method can provide support in locomoting systems over mildly heterogeneous terrain, where individual disturbances can lead to failure [54]. The periodic

tapping strategy consists of tail oscillation from 0° to a β_{set}. Such a scheme results in the tail regularly attempting to impact the ground, possibly resulting in a significant change to the locomotor's kinematic state [55]. A rectangular wave programmed to the robot at the start of each trial dictates the tapping frequency with an example shown in Figure 2.5 B. These frequencies were varied for different β_{set} by changing the space between pulses in the rectangular wave and keeping mark constant at 0.25 s. With this strategy, the tail tapped at the set frequency irrespective of whether it made ground contact, thus serving as a basic open-loop scheme for tail impacting. Load-triggered tapping relies on failure detection to ascertain when to impact the ground. Based on our knowledge of the system, we anticipated a large, sustained increase in the power intake when encountering trapping failures. Thus, when the perceived load on the system exceeded a threshold and stayed above that intensity for a set amount of time, that served as an indication of a trapping event. The tail would then begin to move periodically from 0° to β_{set} at the maximum frequency of 2 Hz. This scheme is illustrated in Figure 2.5 C and it serves as simple form of closed-loop control where the load detection acts as a rudimentary "observer" for the trapping state.

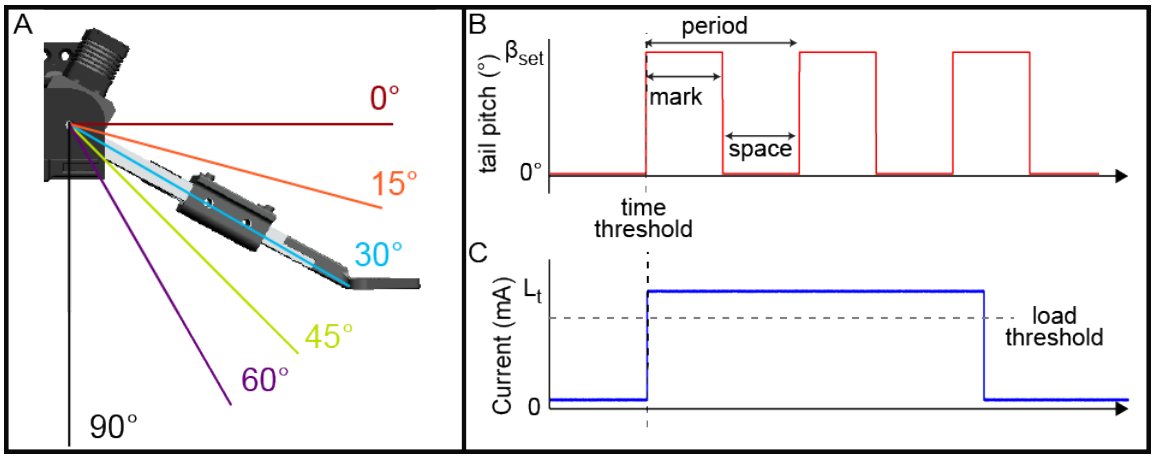

Figure 2.5: **Tail control figure.** (A) Side view of the robot tail with varied tail angle β_{set} - 0° (red line), 15° (orange line), 30° (blue line), 45° (green line), 60° (purple line), and 90° (black line). (B) Diagram showing rectangular wave used to drive periodic tapping. Mark and space are describe the duration of the wave at β_{set} and 0°, respectively. (C) Diagram showing expected behavior of load versus time during a load-triggered behavior.

For all trials detailed in this study, the duty factor d_t of the limbs is set at 75% and the

gait period T_G at 2.5 s. We recorded the robot's path over the terrain via two webcams, a side and a top view. The center of geometry of the robot was tracked via Optitrack and analyzed with custom MATLAB functions. Tailed trials where the robot went off the sides of the course were discarded and tests were terminated once the system achieved a displacement of 140 cm. The locomotor's heading was not actively controlled as the goal was to study the emergent properties of the walker. Trials were conducted until at least 4 tests (maximum of 17) were obtained for a tail behavior where the robot did not fall off the course or suffer damage. We examined the likelihood of traversal by plotting each behavior's empirical complementary cumulative distribution function (eCCDF) of the final displacement from each trial. The mean displacement before failure (MDBF) was obtained by integrating the curve of the CCDF. In addition, we calculated the probability of freeing by taking into account each trapping and freeing event. This was done by analyzing the recorded webcam videos and searching for instances of trapping where the robot had little to no displacement amongst the obstacles for 2 gait cycles (5 seconds for this study). From this data, the probability of freeing was calculated by subtracting the last trapping event (where the robot failed, if applicable) from the total number of times the robot was stuck. Then, the value was divided by the total number of trapping events. These metrics serve as an indication for the tested behavior's ability to mitigate this form of failure while maintaining simple control for the limbs.

CHAPTER 3
RESULTS AND DISCUSSION

3.1 Note to the reader

The figures and data presented in this chapter correspond to work published in *Robotics for Sustainable Future: CLAWAR 2021* under the title *Enhancing Legged Robot Navigation of Rough Terrain via Tail Tapping* [71]. The publisher is not responsible for any errors or omissions in this version of the manuscript or any version derived from it. The Version of Record is available online at https://doi.org/10.1007/978-3-030-86294-7_19 and at https://crablab.gatech.edu/pages/publications/index.html.

3.2 Robot performance without tail

We first tested the robophysical model without a tail using a diagonal couplet gait (Figure 2.2 B) over a flat surface and the rough terrain. Snapshots of the robot's progression over time is shown in Figure 3.1 A&B for these two surfaces. The robot was able to traverse the flat course with a periodic oscillation in its displacement over time, shown in Figure 3.1 C. On the rough terrain (Figure 3.1 D), the displacement versus time does not display any significant periodicity and instead, there are portions of time where the displacement plateaus. This region emerges when the robot is trapped in the terrain. For the case presented, this plateau occurs at the 10 second mark and remains for 5 seconds. At this point, a limb was unable to complete a rotation within 2 gait cycles and so the kill switch was triggered. This results in the robot "relaxing" which is why there is a change in the displacement after the 15 second mark.

We then ran the robot across those two surfaces with different gait patterns where we varied the phasing between the limbs. Example trajectories for the gaits (pace, single foot, trot, pronk, and bound) are shown in Figure 3.2 A&B for flat and rough terrain, respectively.

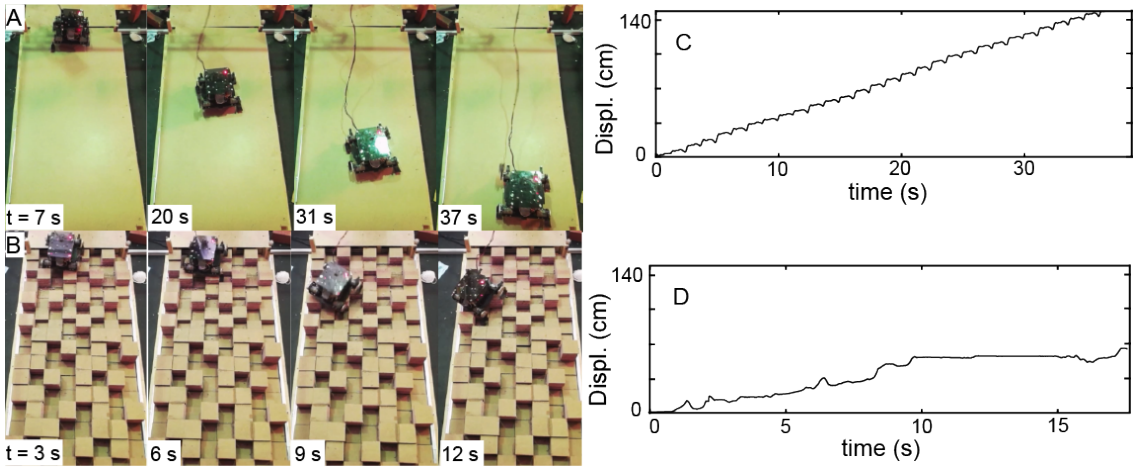

Figure 3.1: **Example gait trial over flat and rough terrain.** Snapshots of the robot moving over a flat (A) and rough (B) terrain, using the diagonal couplet. Example displacement over time for the robot using the diagonal couplet gait over flat (C) and rough (D) terrain.

The phase parameters used to distinguish the different patterns and the colors associated with each gait are shown in the boxes to the right of Figure 3.2. On the flat surface, the robot was able to traverse the course independent of the prescribed gait. With the diagonal couplet and pronk gait, the robot reached the end of the course consistently, evidenced by the flat lines at the 140 cm mark in the displacement box plot for flat ground shown in Figure 3.2 C. However, the pronking gait is one where all legs move simultaneously and so, there are significant vertical oscillations and power consumption associated with such a pattern that are not shown in this figure. With the other gaits, the robot did not move in a straight path over the flat course and fell off the sides. As expected, for the different gaits, the system did not exhibit any trapping or locomotor failure over the flat ground. However, the robot was consistently hindered from traversing the rough terrain. It encountered traps that resulted in median displacements of 35.4 cm, 39.6 cm, 37.5 cm, 29.1 cm, 59.1 cm, and 34.3 cm for the pace, single foot, diagonal couplet, trot, pronk, and bound gait, respectively. A box plot in Figure 3.2 C shows the difference in performance across the two courses. This method of data representation was used since the underlying failure distribution is unlikely to be Gaussian and so, the quantiles represent the spread of the data more effectively. As is evidenced in Figure 3.2 C, the rough terrain trials had significantly lower displacements

than their flat terrain counterparts due to the traps, despite including tests that went over the sides of the course.

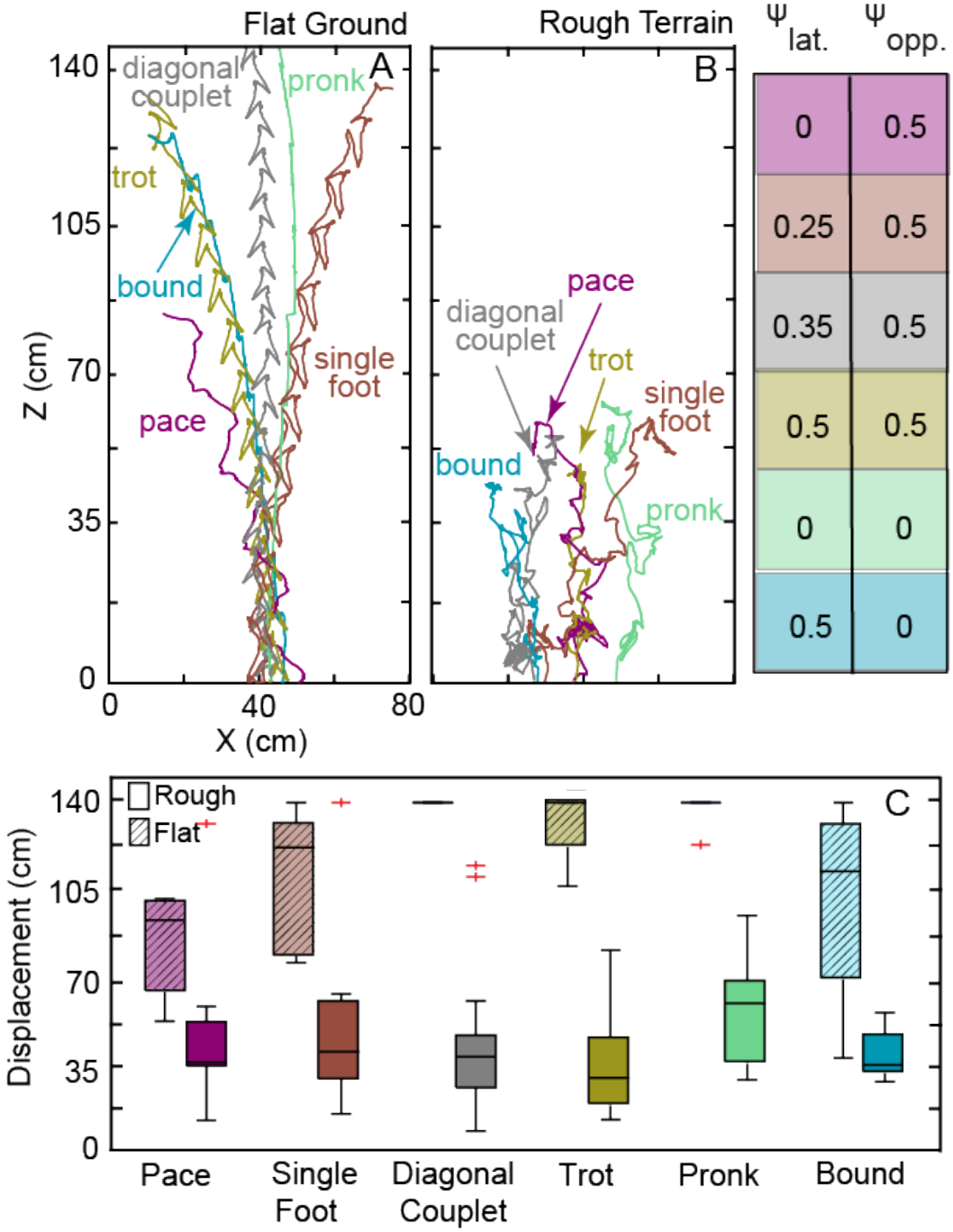

Figure 3.2: **Gait trials over flat and rough terrain.** Example trajectories for each gait over flat (A) and rough (B) terrain. Gaits tested were pace (purple), single foot (burgundy), diagonal couplet (gray), trot (gold), pronk (turquoise), and bound (blue). (C) Median displacement per gait over flat and rough terrain. Red crosses show outliers. Phase shift between lateral (ψ_{lat}) and opposite (ψ_{opp}) limbs for each gait are shown to the right.

The discrepancy between the flat and rough terrain displacements is due to the difference in propulsion methods. Over the flat ground, the limbs provide thrust to the overall body by generating force that is in the direction of travel by interacting with a horizontal surface ("floor"). This force is mainly in the form of Coulomb friction with some additional impulses from when a limb initially impacts the ground. However, over the rough terrain, the limbs have a second means of providing body thrust by pushing off of the vertical planes ("walls") present. Thus, there are instances of "obstacle-aided" propulsion where the robot achieves higher instantaneous velocities than it could on flat ground. Ordinarily, this would serve as a significant form of perturbation to the stability of the locomotor since it corresponds to a removal of a supporting force. However, when on the rough terrain, the robot's belly is mainly in contact with the ground. This is quite different than the case on flat ground where the robot's underside is mainly suspended in air. By keeping the belly in contact with the ground, the underside acts as another point of support over the rough terrain.

Acknowledging this obstacle-aided propulsion and the belly as a point of support is key to understanding how trapping failures occur within this system. This propulsion against walls does not have any compliance, unlike the method over floors which can shift from static to kinetic friction (slip). In this open-loop system, the limbs rotate regardless of whether there has been a body collision that halts forward motion. For the case where slip occurs, the limbs continue to rotate without significant impedance, preventing the actuators from over-torquing. In the case where slip does not occur, a trap will ensue since the robot will damage itself through motor or pitch-back failure in attempting to rotate the legs. For the current system, the traction on the limbs is such that slipping occurs before failure. With the obstacle-aided method, there is no such compliance. Therefore, if the robot is impeded when using this scheme, a limb will continue increasing its torque until the motor fails. Instances like this are common on the rough terrain course since the belly acts as an extra point of support and as an additional point to impede motion. To escape these traps, the "pushing limb" could continue to increase its torque and propelling force until

the body pushes through the obstacle, effectively remodeling its environment. However, such a method is not possible on this created terrain. Therefore, the only remaining way for the robot to escape from a trap is by removing the pushing limb's frictional foothold. This can be done by the individual motor increasing its torque until it surpasses the static friction limit against the wall or by one of the other limbs pushing the body such that the same effect is achieved. This serves as an indication that adding a tail could offer a benefit to the locomotor by offering additional methods through which to remove the frictional foothold.

3.3 Tailed robot performance over rough ground

For all tail strategies, the robot used the diagonal couplet gait as it was the only gait that remained within the course bounds and reached the end of the course consistently while having minimal vertical oscillations and power consumption. Additionally, only the pitch servo (along the vertical plane) was active and the yaw servo (along the horizontal plane) was free to move passively. Displacement analysis was performed only on the trials that remained within the course for the entire experiment, ending when a trap fully halted the robot or the locomotor surpassed 140 cm. The diagonal couplet median displacement and MDBF is thus changed from 37.5 cm and 41.0 cm to 30.6 cm and 39.8 cm, respectively.

3.3.1 Static tail strategy

For the static tail strategy, we tested four β_{set} angles: 0°, 15°, 30°, and 45°. This method was inspired by Tailbot [54] and serves as the simplest way to use an active tail. Figure 3.3 A shows sample trajectories for each angle with the associated displacement over time plots in Figure 3.3 B-E. Within these example trials, we see plateaus in the displacement that correspond to instances of trapping, with the final instance being marked here by the dashed black line.

The 0° static tail trials probe the effect that this appendage has on the overall system due to its added mass and geometry. The tail's inclusion hinders the robot's ability to traverse

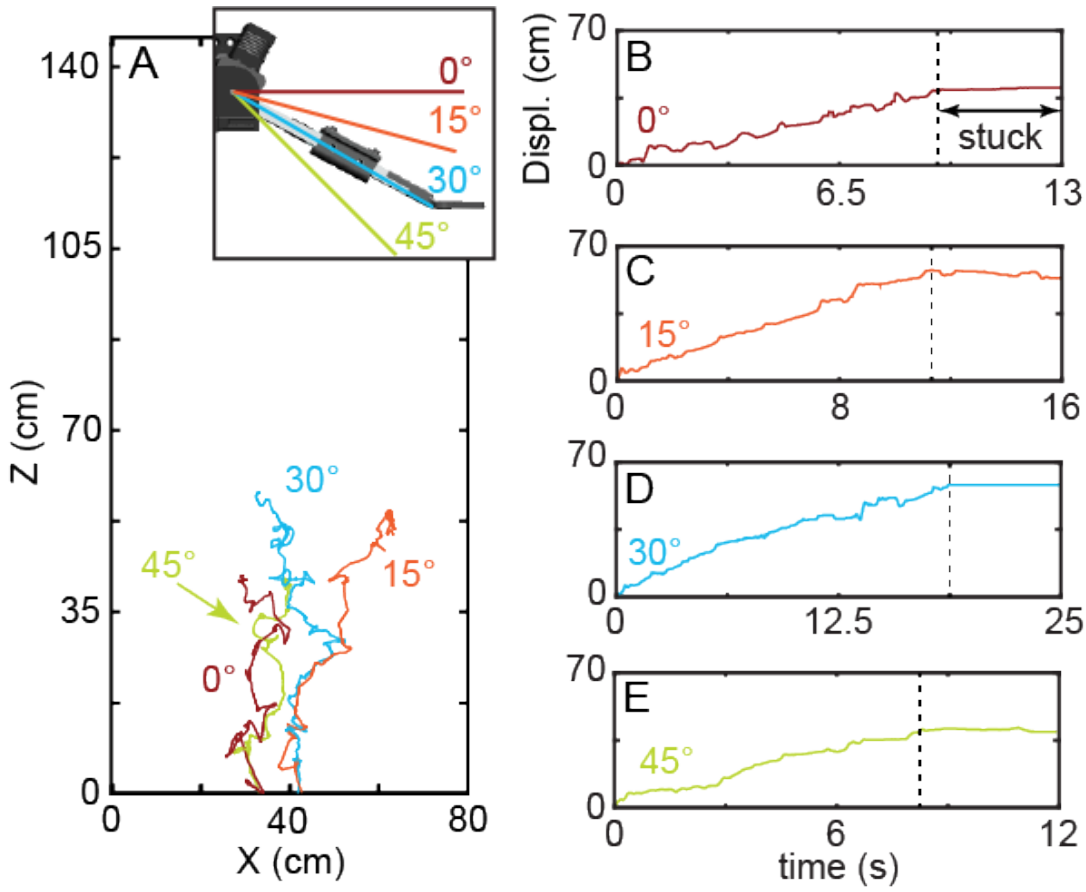

Figure 3.3: **Static tail strategy examples.** (A) Example trajectories over rough terrain for each angle tested: 0° (red), 15° (orange), 30° (blue), and 45° (green). Example displacements versus time for β_{set} of (B) 0°, (C) 15°,(D) 30°, and (E) 45°. Black lines indicate where the final trapping event occurred.

the course, lowering its survival likelihood for long distances, as seen in the eCCDF in Figure 3.4 A as well as the MDBF being 34.3 cm (lower than the no tail version). Furthermore, the robot's probability of freeing was reduced from 0.25 to 0.125 as seen in Figure 3.4 B. The 15° tail strategy had similar effects on the locomotor, reducing the long distance likelihood with an MDBF of 49.1 cm. This signifies an increase in the average distance traveled along with a reduction in the survival likelihood for long distance. This is due to the 15° trials tending to fail within a certain region on the course, rather than failing more spread out like in the no tail trials. Additionally, this behavior decreased the probability of freeing further to 0.08. These reductions in freeing ability were due to the added mass causing the robot to tend to pitch backwards as it encountered obstacles and the geometry of the tail

preventing the system from pitching like it desired. This served as another impediment for the robot's motion and thus induced trapping more often without a means of eliminating the frictional foothold, resulting in the aforementioned reductions in locomotor performance.

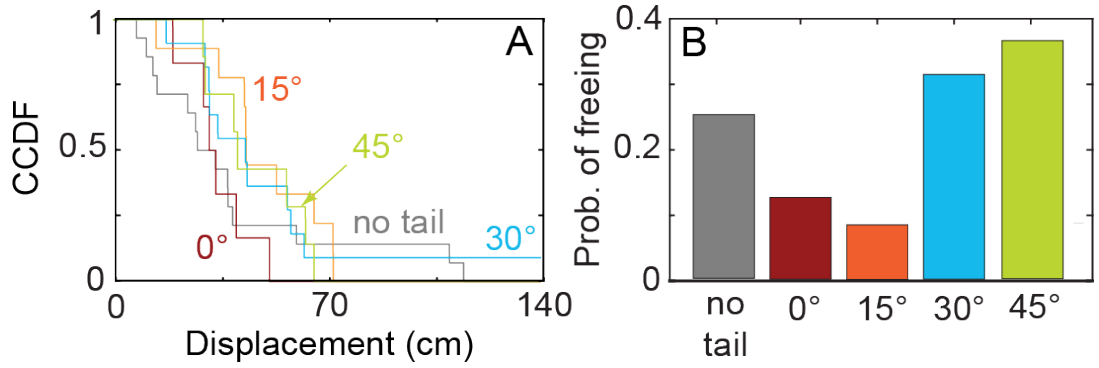

Figure 3.4: **Static tail strategy summary.** (A) Empirical complementary cumulative distribution functions (eCCDFs) and (B) probability of freeing for each tested angle and the robot without the tail (gray).

When at higher angles like 30° and 45°, the weight-induced pitching of the robot was mitigated by the additional point of support offered by the tail. Furthermore, this additional contact reduced the likelihood for the back limbs to fall deeply into holes and thus, they were not as strongly held by these obstructions. This resulted in higher freeing probabilities for these angles as seen in Figure 3.4 B with the 30° and 45° tail trials having freeing likelihoods of 0.31 and 0.36 with MDBFs of 50.0 cm and 46.5 cm, respectively. The 30° static tail behavior also showed an improved long distance survival likelihood when compared to the no tail experiments while the 45° tests showed a reduction in this metric. This was due to the high tail angle pushing the front of the robot further down, making it more likely to collide with obstacles in the terrain. Additionally, this behavior exposed more of the tail to the terrain at large impact angles, making snags more common despite the design elements to mitigate such effects (see Figure 2.4 C). These trials and results hint at the need for more dynamic behaviors to mitigate trapping. A static element simply changes the terrain-locomotor configuration at which trapping occurs and does not introduce the dynamics necessary.

3.3.2 Periodic tapping strategy

For the second tail strategy, we tested periodic open-loop tapping where β_{set} oscillated from 0° to one of three angles: 15°, 30°, and 45°. A high and a low frequency was tested per angle. This served to gauge the effects that tap amplitude and timing had on the robot's performance. For each angle, the high frequency test was the max frequency possible (2 Hz). A different low frequency was used for each angle to account for the changed amplitudes with 15°, 30°, and 45° having frequencies of 0.67, 0.33, and 0.22 Hz, respectively. Example trajectories for these behaviors are shown in Figure 3.5 A&B with corresponding displacement over time in Figure 3.5 C-E. Across all angles tested, the lower frequency tapping outperformed its high frequency counterpart in distance traveled, with more variation in the freeing likelihood across these two behaviors.

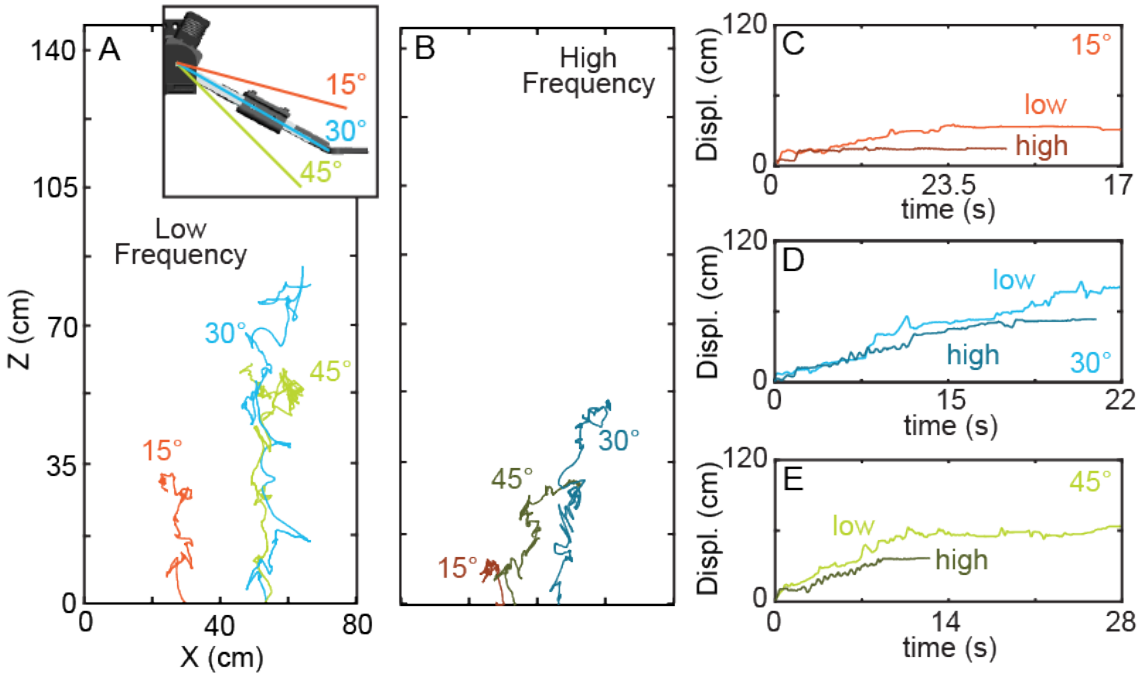

Figure 3.5: **Periodic tapping strategy examples.** Example trajectories over rough terrain for periodic tapping at (A) low and (B) high frequency. Inset in (A) shows angles tested: 15° (orange), 30° (blue), and 45° (green). Higher frequency colored with a darker shade of the assigned color. Example periodic tapping displacements versus time for (C) 15°,(D) 30°, and (E) 45°.

During the 15° tests, we observed similar effects to those detailed in the static angle

tests. Namely, the robot's ability to free itself was reduced to 0.11 and 0.17 for low and high frequencies, respectively. Moreover, at these lower amplitudes, the survival likelihood in Figure 3.6 A&B was reduced and the MDBFs became 37.3 cm and 22.3 cm for the low and high frequencies, respectively.

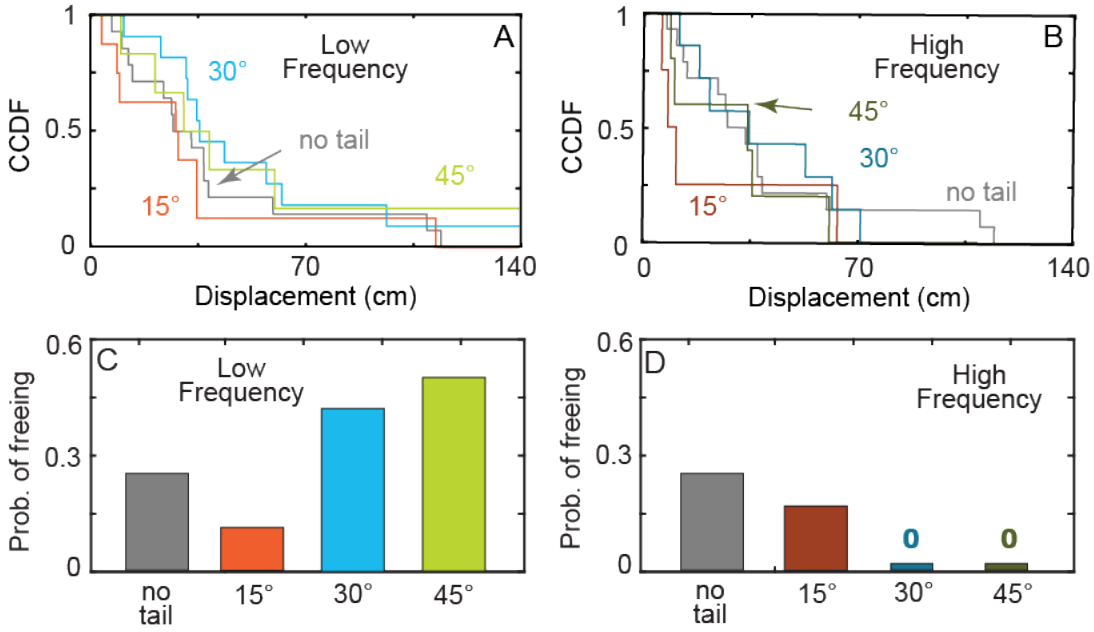

Figure 3.6: **Periodic tapping strategy summary.** eCCDFs for tested angles in (A) low and (B) high frequency with the robot without the tail (gray). Probability of freeing for each angle for low (C) and high frequency (D).

When at more significant amplitudes, both methods of periodic tapping served to effectively disrupt the kinematic state of the robot relative to the terrain, removing the friction foothold on the trapped limb. However, with the high frequency trials, the robot's performance was hindered due to this disruption. The 30° and 45° tapping behaviors affected the system's heading, leading to several trials being discounted as the robot fell off the sides of the course. These trials shown in Figure 3.6 B have a low survival likelihood for long distances, as well as MDBFs of 39.0 cm and 30.1 cm for 30° and 45°, respectively. This tapping behavior tended to cause the robot to escape potential failure regions for the back limbs before the requisite 5 seconds passed for that event to be logged as a "trap". However, when the system did fall into a trap, this high frequency tapping prevented the robot from freeing itself, leading to the low probability of freeing shown in Figure 3.6 D. This was due

to the impacts causing the overall locomotor to pitch forward and drive the front limbs and belly deeper into the terrain. Consequently, those limbs tended to become trapped more often with these high amplitude taps preventing other legs from getting the sufficient traction to free the system. Additionally, the tail pushed the body backwards, driving trapped limbs further into obstacles. From these tests, it is evident that disrupting the kinematic state of the robot can hinder its performance if done extensively and improperly.

When at lower frequencies, high amplitude tapping improved locomotor performance. The 30° and 45° tapping trials had improved long distance survival and MDBFs of 52.1 cm and 50.6 cm, respectively (see Figure 3.6 A). Additionally, these behaviors improved the likelihood of freeing from 0.25 to 0.42 and 0.50, as seen in Figure 3.6 C. At these angles, the tail made consistent contact with the ground, which was the major failing of the 15° tapping behaviors. Additionally, the tail tended to hit the ground when the robot was on the verge of failure, leading to the higher freeing probability. Notably, the system often landed into a new trapping region after the initial tap freed it. Consequently, the robot typically reached the kill condition before a new series of taps could be performed that freed it. The improvement observed with these tests suggests that the optimal timing of tail impacts changes based on the kinematic state of the robot and the local terrain conditions. Therefore, while proper tapping can improve performance, an open-loop method is unlikely to consistently mitigate trapping failures.

3.3.3 Load-triggered tapping

For the final tail strategy, we applied a closed-loop method for tapping to the system. In this behavior, the tail would begin to tap at 2 Hz once the detected current on the power supply exceeded a threshold of 2.5 amps for more than 100 milliseconds. Once started, the tail would continue to tap until the load dropped below the baseline, after which the appendage finished its last cycle before resting (see Figure 2.5 B&C). This strategy builds off of the knowledge acquired in the open-loop tapping tests. Namely, that the timing of the taps plays an important role in how the behavior affects the locomotor performance. If

done too often, the impacts hinder the robot as seen in the high frequency tapping tests. If done too intermittently, the robot is likely to fail before another tail impact can free it. We tested three β_{set} angle amplitudes: 30°, 60°, and 90°. Example trajectories for each can be seen in Figure 3.7 A with associated displacements over time in Figure 3.7 B-D.

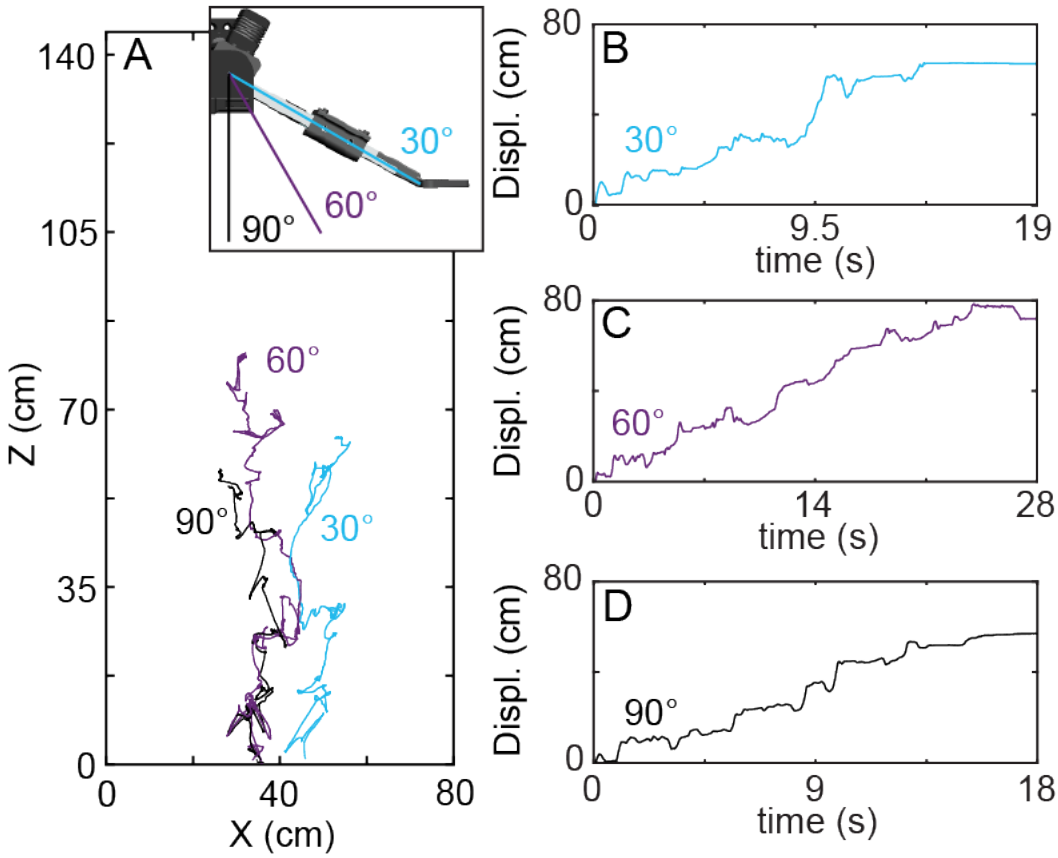

Figure 3.7: **Load-triggered tapping strategy examples.** (A) Example trajectories over rough terrain for each angle tested for the load-triggered behavior. Inset illustrates tail angles tested: 30° (blue), 60° (purple) and 90° (black). Example displacements versus time for (B) 30°, (C) 60°, and (D) 90°.

This strategy managed to consistently address trapping as it occurred, with examples shown in Figure 3.7 B-D at 9.5 sec, 12 sec, and 9 sec, respectively. This improvement resulted in the likelihood of terrain traversal being comparable to or greater than the robot without the tail (Figure 3.8 A). Each amplitude increased MDBF and freeing probability from 39.8 cm and 0.25 for the no tail trials to 45.3 cm, 67.1 cm, and 50.3 cm and 0.28, 0.40, and 0.35 for the 30°, 60°, and 90° angles, respectively. Additionally, these angles improved

survival likelihood for the entire course, with 60° having the best enhancement. With the 30° amplitude trials, the tail offered only minor benefits to the robot since the impacts did not consistently provide sufficient force to free the system. At the 90° amplitude, the tail would over-disrupt the locomotor like in the 30° and 45° high frequency trials. Consequently, the robot would change its heading and take more circuitous routes, increasing the likelihood to fall into traps where tail-ground contact was not guaranteed. With 60° load-triggered tests, the locomotor had the most improvement since the taps disrupted the system enough to free it without significantly affecting the heading. This meant that the robot traveled relatively straight and when traps were encountered, it often had tail-ground contact possible.

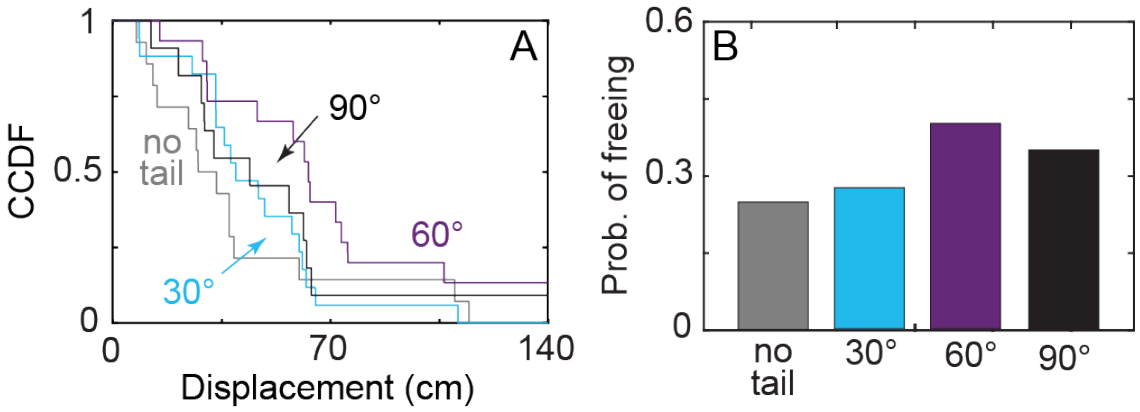

Figure 3.8: **Load-triggered tapping summary.** (A) eCCDFs for each tested angle and the robot without the tail (gray). (B) Probability of freeing for each angle.

3.3.4 Tailed strategy summary

Comparing across all tested behaviors, low frequency periodic tapping at β_{set} of 30° and 45° outperformed other strategies in the likelihood of freeing as seen in Figure 3.9 A. However, this periodic strategy is not easily applied outside of a lab setting. In reality, the robot only needs to tap momentarily to free itself from a trap. Disruptions brought on by further tapping could hinder performance over less hazardous areas. In contrast, load-triggered tapping and a static tail both offer real-world applicability. For the static tail, the median distance traveled increased from 30.6 cm to 43.6 cm and 43.4 cm for 30° and

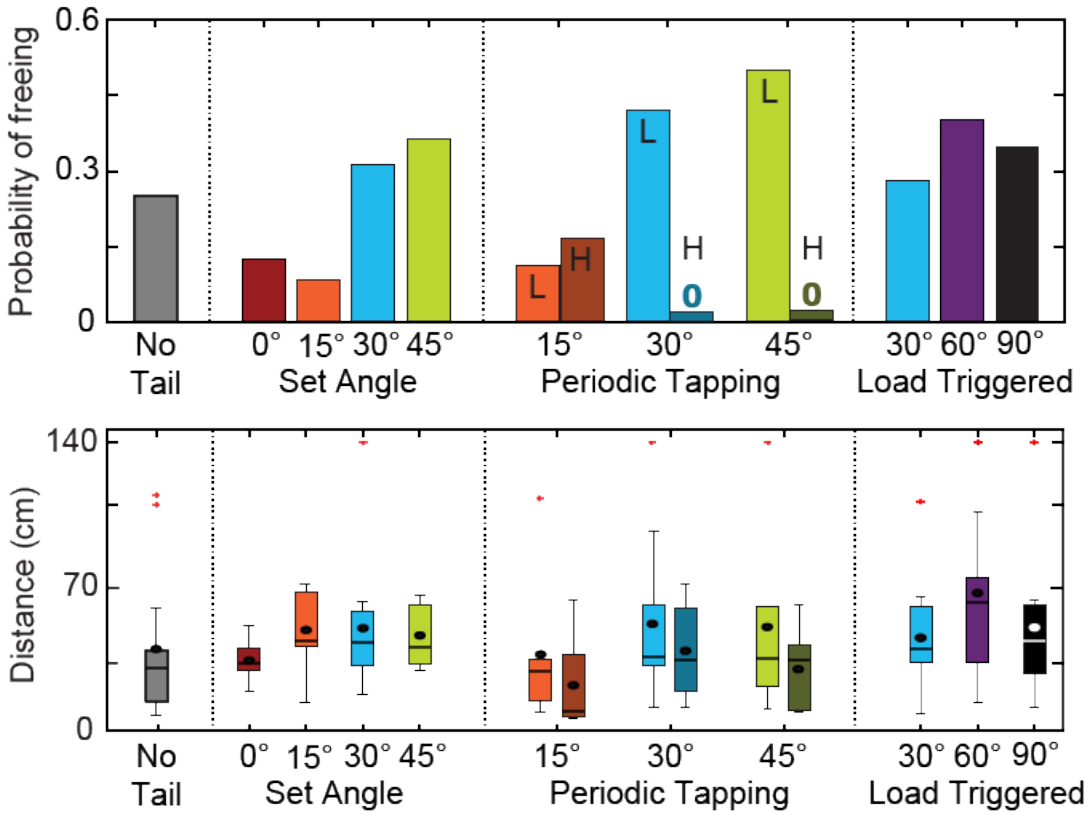

Figure 3.9: **Tail strategies comparison.** (A) Probability of freeing for each behavior. (B) Median displacement for each tail behavior. Black/white dots show the mean displacement before failure (MDBF). Black/white horizontal lines show the median. Red crosses show outliers. Statistic performed with a Wilcoxon rank sum test, comparing each behavior. Differences were significant at $p \leq 0.05$ when comparing load-triggered 60° to low frequency 15°, high frequency 15°, and high frequency 45°.

45°, respectively. This behavior can also offer benefits in homogeneous or less hazardous environments by stabilizing the system through a new point of support [54]. While not providing the best improvement for probability of freeing, load-triggered tapping offered consistent performance in that metric across all angles tested. Furthermore, this behavior had the best improvement in both the average and median distance traveled. This indicates that the tail strategy improved the locomotor more consistently than the other behaviors and thus, it can serve as a desirable strategy for field robotics. The 60° tapping behavior had the most improvement with a median distance of 63.0 cm and this was due to the tail consistently making ground contact while not over-disrupting the system like in the 90° trials. The key benefit of this behavior is that it only begins to tap once a "failure"

threshold is met and that offers the possibility for future enhancement through more “failure observers” that do not disturb the robot in less hazardous environments.

CHAPTER 4
CONCLUSION AND FUTURE WORK

Humans wish to apply robots to explore and traverse all types of environments. To achieve this, roboticists have created several locomotor designs that can move over most terrains using different control schemes. However, in certain scenarios, the applied robot has dimensions that are of comparable size to the obstacles and holes present in the environment. In such situations, trapping can occur where the locomotor is unable to make any forward progress due to a limb being trapped in the terrain. When faced with these traps, biological systems utilize their vast array of sensors to detect which limb is at fault and use complex dynamics to free their compliant bodies. Rather than implement such a strategy on an artificial system, could a new mechanism in the form of a tail be introduced to offload the complexity required of the limb control? To probe this question, we performed a robophysical study using a RHex-inspired quadrupedal system with an attachable active tail traversing a terrain designed to elicit failure.

This robot design used a single motor and absolute encoder for each limb and was able to emulate different gaits to walk over flat ground. The robot was able to achieve these different gait patterns via a cascaded series of PID loops on each limb, along with a state feedback control scheme that was inspired by reflex chains observed in simple organisms and robots. This control scheme was able to emulate the desired gait pattern and strictly follow it. This can serve as a point of study for future researchers to gain insight into gait terradynamics over terrains that induce motor stalling. To elicit trapping failures, a complex terrain stepfield was created where the block heights varied according to an inverted normal distribution. Such a distribution, when patterned correctly, was able to bring the robot's motion to a standstill at different points within the terrain.

These diverse and situational terradynamic interactions consistently trapped the robot when it attempted to traverse the designed course. Such conditions prove to be challeng-

ing to predict or detect since they depend on both the locomotor state and the properties of the environment at its location. However, a properly-used simply-controlled active tail enhanced the robot's intrinsic capabilities by mitigating the influence of such interactions. Consequently, the tail improved the traversal likelihood and freeing probability. Additionally, improper tail usage hindered performance by disrupting the robot's natural ability to handle the environment. As such, there is a nonlinear relationship between tail usage and locomotor performance. By including a sensor on the power line, a rudimentary observer for the robot's "trapping state" was introduced and augmented the active tail "controller" to dictate when to begin impacting the ground while avoiding extraneous disturbances. This strategy improved the likelihood of freeing and the distance traveled over the complex terrain. In summary, an actuated tail with minimal control and sensing can be used to augment existing robots to aid in locomotion over hazardous terrains.

This idea of an "observer" and "controller" for the failure state can be a source of future investigation. For instance, refining the observer's ability to detect more forms of failures such as the robot being flipped onto its back or the limbs no longer contacting the ground and being unable to propel the system. Additionally, improving the tail controller's ability to overcome such failures by actuating the yaw servo and incorporating the existing strain sensor would be a good avenue for future work. For instance, the tail was not always guaranteed to impact the ground when tapping since the robot could be tilted in the roll direction which causes the appendage to deal a glancing blow with the terrain. A solution for this is to incorporate the yaw servo into the tail control scheme and to introduce an "observation" step where the tail sweeps through its achievable angles and looks to see where an appreciable increase in power or tail strain occurs. With that done, the tail could then impact the ground at the desired location and with the appropriate force. Additionally, another improvement to be made is with the tail impact control strategy. As it stands, the current approach is a fairly open-loop method where the tail goes to some preassigned angle to do a tap. A more sophisticated approach would entail using the severity of the trapping event (which can be ascertained from the load readings) to dictate the force needed

to extricate the robot. Then using that knowledge, in conjunction with the predetermined location of the terrain, to specify how fast and how much distance the tail must travel before it impacts the ground in order to successfully free the locomotor. Such a scheme could be deemed an ”impact control” and could have uses beyond locomotion and trapping events to situations where forces are needed that are outside the range of what a quasi-static approach can generate. Additionally, it could serve to further this tapping scheme's applicability to more fragile locomotion systems as it would allow one to specify the upper bound of possible disturbances that can be generated by the uncoordinated tail.

Another possible avenue of future work would be to further probe the capabilities of the RQuad system on different terrains (granular media, slopes, slants, etc.) and to see what is possible if the limbs were to respond in tandem with the tail. For instance, we observed that, at times, the limbs were further driven into the walls of the terrain when the tail impacted the ground and this resulted in the robot staying trapped in the environment. A solution for this would be to cause the limbs to have a load-triggered response as well, where the limbs reverse as the tail makes ground contact. Indeed, preliminary tests showed that this strategy resulted in very few robot trapping failures. However, this strategy also resulted in the robot being diverted off its original trajectory and subsequently falling off the course. So this method, while being robust to trapping failures and having a high probability of freeing, has a low eCCDF due to its inability to traverse the terrain. Therefore, refining this method by introducing methods of steering, either through tail [55] or through gait modifications [72] or a combination of the two, could be a potentially rich source of possible improvements for the RQuad platform and how to negotiate trapping.

Finally, another path for future work would be in developing a systematic way to create these obstacled terrains to better understand trapping and possible ways to predict it. This method of creating stepfields of arbitrary configuration and stiffness, with the ability to measure applied forces and torques, could serve as a huge asset to robophysics and the study of field robotics, as well as improve our understanding of how biological systems operate within different 3D environments.

Appendices

APPENDIX A
GAIT CONTROL

Each limb is controlled to rotate according to an angular trajectory known as the Buehler Clock which consists of a fast and slow region. This trajectory, as a function of position, is shown in Equation 2.1. As a function of time, this motion profile takes the form shown in Equation A.1 where t is the input time modulo T_G (the gait period):

$$f(t) = \begin{cases} \omega_f t & t \leq \frac{\theta_{min}}{\omega_f} \\ \omega_s t + (1 - \frac{\omega_s}{\omega_f})\theta_{min} & \frac{\theta_{min}}{\omega_f} < t \leq \frac{\theta_{min}}{\omega_f} + \frac{\phi}{\omega_s} \\ \omega_f t + (1 - \frac{\omega_f}{\omega_s})\phi & otherwise \end{cases} \tag{A.1}$$

For the robot to walk, the four motors must be phased in time relative to one another in order to achieve a gait pattern as detailed in Figure 2.2. Assuming each limb is driven according to Equation A.1 above, then phasing could be achieved by introducing a delay τ_i in each motor's position function as seen in Equation A.2.

$$\theta_i^* = f(t - \tau_i) \tag{A.2}$$

This delay would be specific to each leg and would be relative to a global clock t shared amongst all the limbs. In practice, however, it was simpler and less sensitive to drift if each limb's setpoint velocity was controlled according to its setpoint position. Consequently, the global clock was no longer needed and the phasing of the limbs became an initial condition that was subject to disturbances. As there is no universal reference to compare against, each motor relied on its relative phasing to the other three to control its own "delay". To do this, each motor's time within its angular cycle was estimated from its position. This is possible since the periodic function detailed in Equation A.1 is bijective (i.e. each point in time corresponds to a unique position). This mapping from position to time was done for

each limb, generating a 4-by-1 vector of time estimates t_{map} shown below.

$$t_{map} = t - \tau = f^{-1}(\theta), \theta = \begin{bmatrix} \theta_1 \\ \theta_2 \\ \theta_3 \\ \theta_4 \end{bmatrix}, \tau = \begin{bmatrix} \tau_1 \\ \tau_2 \\ \tau_3 \\ \tau_4 \end{bmatrix} \tag{A.3}$$

The relative phasing between each motor ψ_{est} was then be estimated by taking the difference between each entry in the t_{map} vector. This was done via multiplication with the 16-by-4 matrix M, shown below using the 4-by-4 ones matrix J_4, the 4-by-4 identity matrix I_4, and the matrix unit $E_{i,j}$ which is a 4-by-4 zero matrix except for a 1 in the i-th row and j-th column.

$$\psi_{est} = Mt_{map}, M = \begin{bmatrix} J_4E_{1,4} - I_4 \\ J_4E_{2,4} - I_4 \\ J_4E_{3,4} - I_4 \\ J_4E_{4,4} - I_4 \end{bmatrix} \tag{A.4}$$

This phase estimate was then compared to the desired phase vector (see section 6.0.3) and this 16-by-1 vector was then multiplied by the transpose of M to create a 4-by-1 "error" term. A control gain K ($K = 1$ for this implementation) was then applied to that error term, resulting in a phase correction vector P which effects the setpoint velocity of each corresponding limb.

$$P = KM^T(\psi^* - \psi_{act}) \tag{A.5}$$

$$\dot{\theta}_i^* = P_i + g(\theta^*) \tag{A.6}$$

APPENDIX B

INVERTED NORMAL DISTRIBUTION EQUATIONS

$$X \sim IN(\mu, \sigma^2, \beta) \tag{B.1}$$

PDF:

$$f(x) = \begin{cases} \frac{\kappa}{\sqrt{2\pi\sigma^2}}(1 - e^{-\frac{(x-\mu)^2}{2\sigma^2}}) & , \ \mu - \beta < x \leq \mu + \beta \\ 0 & , \ otherwise \end{cases} \tag{B.2}$$

CDF:

$$F(x) = \begin{cases} 1 & , \ x > \mu + \beta \\ \frac{\kappa}{\sqrt{2\pi\sigma^2}}(x - \sqrt{\frac{\pi\sigma^2}{2}}\,\text{erf}(\frac{x-\mu}{\sqrt{2\sigma^2}})) + \zeta & , \ \mu - \beta < x \leq \mu + \beta \\ 0 & , \ x \leq \mu - \beta \end{cases} \tag{B.3}$$

Quantile:

$$Q(p) = x, \ \text{s.t.} \ q(x, p) = 0 \tag{B.4}$$

$$q(x, p) = x - \sqrt{\frac{\pi\sigma^2}{2}}\,\text{erf}(\frac{x-\mu}{\sqrt{2\sigma^2}}) + \frac{\sqrt{2\pi\sigma^2}}{\kappa}(\zeta - p)$$

$$\kappa = \frac{\sqrt{\sigma^2}}{\beta\sqrt{\frac{2}{\pi}} - \sqrt{\sigma^2}\,\text{erf}(\frac{\beta}{\sqrt{2\sigma^2}})}$$

$$\zeta = \frac{1}{2} - \frac{\mu}{2\beta - \sqrt{2\pi\sigma^2}\,\text{erf}(\frac{\beta}{\sqrt{2\sigma^2}})}$$

APPENDIX C

EQUATIONS FOR IMPLEMENTATION

Slow and fast velocities used in Buehler Clock:

$$\omega_s = \omega_{slow} = \frac{\phi}{d_t T_G}, \omega_f = \omega_{fast} = \frac{1-\phi}{T_G(1-d_t)}$$

Desired phase between limbs according to a gait pattern:

$$\psi^* = \begin{bmatrix} \psi_1 \\ \psi_2 \\ \psi_3 \\ \psi_4 \end{bmatrix}$$

$$\psi_1 = \begin{bmatrix} 0 \\ \psi_{lat} \\ \psi_{opp} \\ \psi_{lat} + \psi_{opp} \end{bmatrix}, \psi_2 = \begin{bmatrix} -\psi_{lat} \\ 0 \\ \psi_{opp} - \psi_{lat} \\ \psi_{opp} \end{bmatrix}, \psi_3 = \begin{bmatrix} -\psi_{opp} \\ \psi_{lat} - \psi_{opp} \\ 0 \\ \psi_{lat} \end{bmatrix}, \psi_4 = \begin{bmatrix} -(\psi_{lat} + \psi_{opp}) \\ -\psi_{opp} \\ -\psi_{lat} \\ 0 \end{bmatrix}$$

Motor time estimate given position:

$$t_{map,i} = f^{-1}(\theta_i) = \begin{cases} K_1\theta_i & \theta_i < t_{min} \\ K_2\theta_i + K_3 & \theta_{min} \leq \theta_i < \theta_{min} + \phi \\ K_1\theta_i + K_4 & \theta_i \geq \theta_{min} + \phi \end{cases}$$

$$K_1 = \frac{1-d_t}{1-\phi}, K_2 = \frac{d_t}{\phi}, K_3 = \theta_{min}(K_1 - K_2), K_4 = d_t - \phi K_1$$

REFERENCES

[1] S. J. Freedberg, *Why the military wants robots with legs (not to run faster than usain bolt)*, Sep. 2012.

[2] F. Iida and A. J. Ijspeert, "Biologically inspired robotics," in *Springer Handbook of Robotics*, B. Siciliano and O. Khatib, Eds. Cham: Springer International Publishing, 2016, pp. 2015–2034, ISBN: 978-3-319-32552-1.

[3] E. Hoerner, *National park service: Check out devils golf course*, [Online; accessed April 15, 2021].

[4] Epstein, *The buffalo news: Historic chautauqua institution amphitheater demolished into pile of rubble*, [Online; accessed April 15, 2021], Sep. 2016.

[5] NASA, *Pathfinder's rocky terrain*, [Online; accessed April 15, 2021], 1997.

[6] S. D. Frank, *Obsidian dome*, Nov. 2019.

[7] A. M. Johnson, C. W. III, M. Tesch, K. Lipkin, and H. Choset, "A novel architecture for modular snake robots," Carnegie Mellon University, Pittsburgh, PA, Tech. Rep. CMU-RI-TR-11-29, Aug. 2011.

[8] H. Marvi *et al.*, "Sidewinding with minimal slip: Snake and robot ascent of sandy slopes," *Science*, vol. 346, no. 6206, pp. 224–229, 2014.

[9] K. Y. Pettersen, "Snake robots," *Annual Reviews in Control*, vol. 44, pp. 19–44, 2017.

[10] Y. O. Aydin, J. L. Molnar, D. I. Goldman, and F. L. Hammond, "Design of a soft robophysical earthworm model," in *2018 IEEE International Conference on Soft Robotics (RoboSoft)*, 2018, pp. 83–87.

[11] B. Liu, Y. Ozkan-Aydin, D. I. Goldman, and F. L. Hammond, "Kirigami skin improves soft earthworm robot anchoring and locomotion under cohesive soil," in *2019 2nd IEEE International Conference on Soft Robotics (RoboSoft)*, 2019, pp. 828–833.

[12] Y. Ozkan-Aydin, B. Liu, A. C. Ferrero, M. Seidel, F. L. Hammond, and D. I. Goldman, "Lateral bending and buckling aids biological and robotic earthworm anchoring and locomotion," *Bioinspiration & Biomimetics*, vol. 17, no. 1, p. 016 001, Nov. 2021.

[13] D. Koh, J. Yang, and S. Kim, "Centipede robot for uneven terrain exploration: Design and experiment of the flexible biomimetic robot mechanism," in *2010 3rd IEEE*

RAS EMBS International Conference on Biomedical Robotics and Biomechatronics, 2010, pp. 877–881.

[14] O.-A. et al., "A systematic approach to creating terrain-capable hybrid soft/hard myriapod robots," in *2020 3rd IEEE International Conference on Soft Robotics (RoboSoft)*, IEEE, 2020, pp. 156–163.

[15] Y. Ozkan-Aydin and D. I. Goldman, "Self-reconfigurable multilegged robot swarms collectively accomplish challenging terradynamic tasks," *Science Robotics*, vol. 6, no. 56, eabf1628, 2021.

[16] D. Kerimoglu, M. Karkoub, U. Ismail, O. Morgul, and U. Saranli, "Efficient bipedal locomotion on rough terrain via compliant ankle actuation with energy regulation," *Bioinspiration &amp Biomimetics*, vol. 16, no. 5, p. 056 011, Aug. 2021.

[17] S. et al., "Rhex: A simple and highly mobile hexapod robot," *IJRR*, vol. 20, no. 7, pp. 616–631, 2001.

[18] P. Wensing, "The rapid rise of quadruped robots [young professionals]," *IEEE Robotics Automation Magazine*, vol. 28, no. 3, pp. 168–168, 2021.

[19] R. McGhee and A. Frank, "On the stability properties of quadruped creeping gaits," *Mathematical Biosciences*, vol. 3, pp. 331–351, 1968.

[20] J. L. Callas, "Mars exploration rover spirit end of mission report," Tech. Rep., 2015.

[21] F. Rubio, F. Valero, and C. Llopis-Albert, "A review of mobile robots: Concepts, methods, theoretical framework, and applications," *International Journal of Advanced Robotic Systems*, vol. 16, no. 2, p. 1 729 881 419 839 596, 2019.

[22] R. et al., "A controller for the littledog quadruped walking on rough terrain," in *Proceedings 2007 IEEE International Conference on Robotics and Automation*, 2007, pp. 1467–1473.

[23] E. Tennakoon, T. Peynot, J. Roberts, and N. Kottege, "Probe-before-step walking strategy for multi-legged robots on terrain with risk of collapse," in *2020 IEEE International Conference on Robotics and Automation (ICRA)*, 2020, pp. 5530–5536.

[24] B. Dynamics, *Spot*, [Online]. Available: https://www.bostondynamics.com/spot, May 2021.

[25] B. Dyamics, *Atlas*, [Online]. Available: https://www.bostondynamics.com/atlas, May 2021.

[26] J. Lee, S. N. Sponberg, O. Y. Loh, A. G. Lamperski, R. J. Full, and N. J. Cowan, "Templates and anchors for antenna-based wall following in cockroaches and robots," *IEEE Transactions on Robotics*, vol. 24, no. 1, pp. 130–143, 2008.

[27] H. Cruse, T. Kindermann, M. Schumm, J. Dean, and J. Schmitz, "Walknet—a biologically inspired network to control six-legged walking," *Neural Networks*, vol. 11, no. 7, pp. 1435–1447, 1998.

[28] C. Ferreira, J. Figueiredo, and C. P. Santos, "Quadruped locomotion based on central pattern generators and reflexes," in *2015 IEEE International Conference on Autonomous Robot Systems and Competitions*, 2015, pp. 29–34.

[29] A. Cangelosi, J. Bongard, M. H. Fischer, and S. Nolfi, "Embodied intelligence," in *Springer Handbook of Computational Intelligence*, J. Kacprzyk and W. Pedrycz, Eds. Berlin, Heidelberg: Springer Berlin Heidelberg, 2015, pp. 697–714, ISBN: 978-3-662-43505-2.

[30] G. Loeb, "Control implications of musculoskeletal mechanics," in *Proceedings of 17th International Conference of the Engineering in Medicine and Biology Society*, vol. 2, 1995, 1393–1394 vol.2.

[31] I. E. Brown and G. E. Loeb, "A reductionist approach to creating and using neuromusculoskeletal models," in *Biomechanics and Neural Control of Posture and Movement*, J. M. Winters and P. E. Crago, Eds. New York, NY: Springer New York, 2000, pp. 148–163, ISBN: 978-1-4612-2104-3.

[32] X. Zhou and S. Bi, "A survey of bio-inspired compliant legged robot designs," *Bioinspiration & Biomimetics*, vol. 7, no. 4, p. 041 001, Nov. 2012.

[33] A. Gupta, S. Savarese, S. Ganguli, and L. Fei-Fei, "Embodied intelligence via learning and evolution," *Nature Communications*, vol. 12, no. 1, p. 5721, Oct. 2021.

[34] R. Full and D. Koditschek, "Templates and anchors: neuromechanical hypotheses of legged locomotion on land," *Journal of Experimental Biology*, vol. 202, no. 23, pp. 3325–3332, Dec. 1999. eprint: https://journals.biologists.com/jeb/article-pdf/202/23/3325/1235972/3325.pdf.

[35] R. Full, K. Autumn, J. Chung, and A. Ahn, "Rapid negotiation of rough terrain by the death-head cockroach," *American Zoologist*, vol. 38, no. 5, 81A, 1998.

[36] Sponberg and Full, "Neuromechanical response of musculo-skeletal structures in cockroaches during rapid running on rough terrain," *JEB*, vol. 211, no. 3, pp. 433–446, 2008.

[37] M. et al., "Reliable stair climbing in the simple hexapod 'rhex'," in *Proceedings 2002 IEEE International Conference on Robotics and Automation*, vol. 3, 2002, 2222–2227 vol.3.

[38] S. et al., "Distributed mechanical feedback in arthropods and robots simplifies control of rapid running on challenging terrain," *Bioinspiration & biomimetics*, vol. 2, no. 1, p. 9, 2007.

[39] H. Chang, J. Chang, G. Clifton, and N. Gravish, "Anisotropic compliance of robot legs improves recovery from swing-phase collisions," *Bioinspiration & Biomimetics*, vol. 16, no. 5, p. 056 001, Aug. 2021.

[40] C. Li, A. O. Pullin, D. W. Haldane, H. K. Lam, R. S. Fearing, and R. J. Full, "Terradynamically streamlined shapes in animals and robots enhance traversability through densely cluttered terrain," *Bioinspiration & Biomimetics*, vol. 10, no. 4, p. 046 003, Jun. 2015.

[41] Y. Han *et al.*, "Shape-induced obstacle attraction and repulsion during dynamic locomotion," *The International Journal of Robotics Research*, vol. 40, no. 6-7, pp. 939–955, 2021. eprint: https://doi.org/10.1177/0278364921989372.

[42] Schiebel and M. et al., "Robophysical modeling of bilaterally activated and soft limbless locomotors," in *Conference on Biomimetic and Biohybrid Systems*, Springer, 2020, pp. 300–311.

[43] T. Wang, J. Whitman, M. Travers, and H. Choset, "Directional compliance in obstacle-aided navigation for snake robots," in *2020 American Control Conference (ACC)*, 2020, pp. 2458–2463.

[44] R. Murphy, *Personal communication*, 2021.

[45] S. Shrivastava *et al.*, "Material remodeling and unconventional gaits facilitate locomotion of a robophysical rover over granular terrain," *Science Robotics*, vol. 5, no. 42, eaba3499, 2020.

[46] B. Zhong *et al.*, "A hierarchical geometric framework to design locomotive gaits for highly articulated robots," Jun. 2019.

[47] Y. Tang *et al.*, "Leveraging elastic instabilities for amplified performance: Spine-inspired high-speed and high-force soft robots," *Science Advances*, vol. 6, no. 19, eaaz6912, 2020.

[48] B. et al., "Tails in biomimetic design: Analysis, simulation, and experiment," in *2012 IEEE/RSJ International Conference on Intelligent Robots and Systems*, 2012, pp. 1473–1480.

[49] A. Jusufi, D. I. Goldman, S. Revzen, and R. J. Full, "Active tails enhance arboreal acrobatics in geckos," *Proceedings of the National Academy of Sciences*, vol. 105, no. 11, pp. 4215–4219, 2008.

[50] S. W. Gart, C. Yan, R. Othayoth, Z. Ren, and C. Li, "Dynamic traversal of large gaps by insects and legged robots reveals a template," *Bioinspiration & Biomimetics*, vol. 13, no. 2, p. 026 006, Feb. 2018.

[51] P. et al., "Dynamic turning of 13 cm robot comparing tail and differential drive," in *2012 IEEE International Conference on Robotics and Automation*, 2012, pp. 5086–5093.

[52] C. et al., "Using an inertial tail for rapid turns on a miniature legged robot," in *2013 IEEE International Conference on Robotics and Automation*, 2013, pp. 5469–5474.

[53] A. M. Johnson, T. Libby, E. Chang-Siu, M. Tomizuka, R. J. Full, and D. E. Koditschek, "Tail assisted dynamic self righting," in *Proceedings of the Fifteenth International Conference on Climbing and Walking Robots*, Jul. 2012, pp. 611–620.

[54] C.-S. et al., "A lizard-inspired active tail enables rapid maneuvers and dynamic stabilization in a terrestrial robot," in *2011 IEEE/RSJ International Conference on Intelligent Robots and Systems*, 2011, pp. 1887–1894.

[55] Casarez and Fearing, "Steering of an underactuated legged robot through terrain contact with an active tail," in *2018 IEEE/RSJ International Conference on Intelligent Robots and Systems (IROS)*, IEEE, 2018, pp. 2739–2746.

[56] F. Qian and D. Goldman, "Anticipatory control using substrate manipulation enables trajectory control of legged locomotion on heterogeneous granular media," in *Micro- and Nanotechnology Sensors, Systems, and Applications VII*, T. George, A. K. Dutta, and M. S. Islam, Eds., International Society for Optics and Photonics, vol. 9467, SPIE, 2015, pp. 303–314.

[57] B. McInroe *et al.*, "Tail use improves performance on soft substrates in models of early vertebrate land locomotors," *Science*, vol. 353, no. 6295, pp. 154–158, 2016.

[58] X. B. Peng, E. Coumans, T. Zhang, T. E. Lee, J. Tan, and S. Levine, "Learning agile robotic locomotion skills by imitating animals," *CoRR*, vol. abs/2004.00784, 2020. arXiv: 2004.00784.

[59] S. Gangapurwala, M. Geisert, R. Orsolino, M. F. Fallon, and I. Havoutis, "RLOC: terrain-aware legged locomotion using reinforcement learning and optimal control," *CoRR*, vol. abs/2012.03094, 2020. arXiv: 2012.03094.

[60] J. Lee, J. Hwangbo, L. Wellhausen, V. Koltun, and M. Hutter, "Learning quadrupedal locomotion over challenging terrain," *CoRR*, vol. abs/2010.11251, 2020. arXiv: 2010.11251.

[61] J. Aguilar *et al.*, "A review on locomotion robophysics: The study of movement at the intersection of robotics, soft matter and dynamical systems," *Reports on Progress in Physics*, vol. 79, no. 11, p. 110 001, Sep. 2016.

[62] J. Aguilar and D. I. Goldman, "Robophysical study of jumping dynamics on granular media," *Nature Physics*, vol. 12, no. 3, pp. 278–283, Mar. 2016.

[63] V. Linevich, D. Monaenkova, and D. I. Goldman, "Robophysical study of excavation in confined environments," *Artificial Life and Robotics*, vol. 21, no. 4, pp. 460–465, Dec. 2016.

[64] J. Aguilar *et al.*, "Collective clog control: Optimizing traffic flow in confined biological and robophysical excavation," *Science*, vol. 361, no. 6403, pp. 672–677, 2018. eprint: https://www.science.org/doi/pdf/10.1126/science.aan3891.

[65] N. D. Naclerio *et al.*, "Controlling subterranean forces enables a fast, steerable, burrowing soft robot," *Science Robotics*, vol. 6, no. 55, eabe2922, 2021. eprint: https://www.science.org/doi/pdf/10.1126/scirobotics.abe2922.

[66] S.-C. Chen, K.-J. Huang, W.-H. Chen, S.-Y. Shen, C.-H. Li, and P.-C. Lin, "Quattroped: A leg–wheel transformable robot," *IEEE/ASME Transactions on Mechatronics*, vol. 19, no. 2, pp. 730–742, 2014.

[67] Hildebrand, "The quadrupedal gaits of vertebrates," *BioScience*, vol. 39, no. 11, p. 766, 1989.

[68] C. Ferreira., V. Matos., C. P. Santos., and A. Ijspeert., "Quadrupedal locomotion based in a purely reflex controller," in *Proceedings of the 11th International Conference on Informatics in Control, Automation and Robotics - Volume 2: ICINCO,*, INSTICC, SciTePress, 2014, pp. 324–331, ISBN: 978-989-758-039-0.

[69] L. Palmer and M. Palankar, "Blind hexapod walking over uneven terrain using only local feedback," in *2011 IEEE International Conference on Robotics and Biomimetics*, 2011, pp. 1603–1608.

[70] J. et al., "Stepfield pallets: Repeatable terrain for evaluating robot mobility," in *Proceedings of the 8th Workshop on Performance Metrics for Intelligent Systems*, 2008, pp. 29–34.

[71] D. Soto, K. Diaz, and D. I. Goldman, "Enhancing legged robot navigation of rough terrain via tail tapping," in *Robotics for Sustainable Future*, D. Chugo, M. O. Tokhi,

M. F. Silva, T. Nakamura, and K. Goher, Eds., Cham: Springer International Publishing, 2022, pp. 213–225.

[72] C.-d. Zhang and S.-m. Song, "Turning gait of a quadrupedal walking machine," in *Proceedings. 1991 IEEE International Conference on Robotics and Automation*, 1991, 2106–2112 vol.3.